Executive Summary

CAER

A study to determine the importance of alkali promoters (K, Li, Cs, Rb) on an iron catalyst (100Fe:4.5Si) in determining the catalytic activity, selectivity and stability was begun this quarter. The study utilizes medium pressure synthesis conditions to compare the alkali promoters under the same reaction conditions and over a wide range of conversions. The ranking of the alkali promoters for the activity of the Fe catalyst depended on the CO conversion level. At a CO conversion of approximately 20%, the activity of the K and Li promoted catalysts are approximately the same with the Li promoted catalyst being slightly more active. At a CO conversion level of 40%, the K promoted catalyst is much more active. As the CO conversion increases to 60%, the four metals have a similar impact on activity. The selectivity of the products by carbon number is essentially the same for the four promoters studied. The activity for the water-gas-shift reaction depended on the alkali promoter. These data suggest that the Li promoter may produce an Fe catalyst that more closely resembles cobalt in producing less WGS than the "normal" iron catalyst.

A study was begun this quarter to characterize the iron phase changes during FTS using individually relevant conditions. An unpromoted iron catalyst and Fe-Si, Fe-K and Fe-Si-K catalysts were studied in the CSTR's using the same methods. To date, only the Mössbauer results for the unpromoted catalyst are available. Catalyst samples were withdrawn immediately after activation and at 23h, 168h and 453 hr. The Mössbauer results show that parallel to an activity decline, the amount of iron present as χ-Fe_5C_2 declines, until after 453 hrs of FTS, the only phase detected was Fe_3O_4. The data suggests that a steady-state surface carbide phase/Fe_2O_3 core phase is not formed for the unpromoted iron catalyst. Work is continuing with the single

and doubly promoted catalysts to define the role of each promoter in determining the composition of the working catalysts.

The results obtained this quarter for the on-going study of the impact on the reducibility of cobalt by the use of different supports and by the incorporation of different promoters and additives to the supported Co catalysts are reported.

The activity of cobalt catalysts is generally ascribed to the active sites located on the surface of cobalt metal clusters formed after reduction of the oxidic species formed after calcination. However, the reducibility of cobalt catalysts is strongly influenced by the nature of the support and the degree of promotion by additives, which is the focus of this work. In general, a tradeoff exists as one increases the reduction temperature to activate the cobalt catalyst. Although more sites are reduced, cobalt clusters sinter at higher reduction temperatures. Therefore, TPR and hydrogen chemisorption studies should be conducted prior to catalytic testing, in order to determine the appropriate temperature for catalyst activation. In general, the number of active sites available after reduction varies with support, promoter type, and degree of promotion. The reason for deactivation of promoted FTS catalysts is a subject requiring further study. TPR studies suggest that there is a difference in the degree of interaction of the promoter with the cobalt after reaction testing for each promoter. However, further experiments, using such techniques as EXAFS, are necessary to determine the extent of these morphological changes. Not only will EXAFS allow the determination of cluster size, but the local structure surrounding Co, including the promoter interaction, may be quantified for the fresh and spent catalysts.

The addition of Pt or Ru to the support had a similar effect on each of the fresh supported catalysts. All the reduction peak positions shifted markedly to lower temperatures, due to

spillover of H_2 from the reduced promoter to reduce Co oxide species. Of particular importance, peaks attributed to the metal support interaction for Co species on TiO_2 and Al_2O_3 are reduced at much lower temperatures, freeing up the availability of metal sites for reaction. For the case of Re, the reduction of Re occurs at higher temperatures than Pt or Ru. Although the low temperature peaks are not significantly affected, Re still plays a valuable role in reducing the reduction temperature of species for which there is a significant metal-support interaction.

TPR analysis of spent promoted 15%Co/Al_2O_3 catalysts revealed that while observed peaks for Ru and Re promoted catalysts remained shifted to low temperatures, the peaks had shifted substantially to higher temperatures in the case of the Pt catalyst. This suggests that the Co and Pt interaction is rapidly lost under reaction, and may be the reason for the higher observed deactivation rate.

The following discussion describes the work done to enhance the CAER's SBCR system. A 5.08 cm diameter by 2 m tubular reactor had been modified to operate in a Fischer-Tropsch SBCR mode. The previous work had focused primarily on catalyst separation from the wax products. Problems with maintaining a constant catalyst inventory within the reactor have been addressed and design modifications are underway. Heat load/loss calculations have been performed to evaluate the need for cooling with high space velocities.

UC/B

In this reporting period, we have started the preparation of a new series of high surface area catalysts based on K- and Cu-promoted Fe-Zn oxides under different treatment protocols. Various factors that influence the surface area of the catalysts have been examined in order to guide the preparation of high surface area catalysts. Using alcohol instead of water to wash the Fe-Zn precipitates increased their surface area markedly (215 vs 148 m^2/g) because low surface

tension alcohols within intraparticle pores in precipitates inhibit pore mouth pinching during drying. Treatment temperatures play a critical role in determining the ultimate surface area of catalysts. It appears that a suitable treatment temperature is ~300 ºC; these temperatures allow the decomposition of Fe hydroxide while preventing loss of surface area of the resulting Fe oxides due to sintering. Since water evolves during hydroxide decomposition and it can cause catalyst sintering, a high space velocity flow of air is required for treating the catalysts (>2000 h^{-1}). Each impregnation slightly decreased the surface area of Fe-Zn precursors (~10-20%). However, the previous impregnation history on Fe-Zn precursors (impregnation promoters on Fe-Zn hydroxide or on oxide precursors) does not appear to influence the ultimate surface area of promoted Fe-Zn oxides at given treatment temperatures.

The structure, reduction and carburization behavior, and catalytic properties of Fischer-Tropsch synthesis (FTS) on these high surface area catalysts were studied using temperature-programmed reduction and carburization in H_2 and CO. The results showed that alcohol-washed Fe-Zn oxides consist of highly dispersed Fe_2O_3 crystallites, which grow larger as the treatment temperatures increase. High surface area Fe-Zn-K4-Cu2 oxides (Zn/Fe=0.1, K/Fe=0.04, Cu/Fe=0.02) reduce at slightly higher temperatures in H_2, but they reduces and carburizes at lower temperatures (~30 K) in CO than on Fe-Zn-K2-Cu1 oxides (Zn/Fe=0.1, K/Fe=0.02, Cu/Fe=0.01). It appears that the surface K/Cu ratio is slightly higher on Fe-Zn-K4-Cu2 oxides.

CO chemisorption was performed on Fe-Zn-K-Cu oxides after FTS reaction at 250 ºC for 1 h in order to examine the effect of promoters on the adsorption behaviors of Fe oxides. The results show higher amounts of desorbed H_2, CO and CO_2 on Fe-K-Cu oxides (20-50 mmol/g-atom Fe) than on Fe-Zn (5-20 mmol/g-atom Fe), but lower amounts than on Fe-Zn-K-Cu oxides (30-80 mmol/g-atom Fe). This reflects a role of each promoter (Zn, Cu, and K) in leading to the

formation of are responsible for higher surface area Fe carbides, which provide a higher density of binding sites for adsorption and also for FTS. The amount of CO chemisorbed on the catalysts is proportional to the surface area of each samples. The presence of K and Cu significantly increases the reduction and carburization rates of Fe oxides, leading to higher surface area Fe carbides, which provide more sites for CO chemisorption and for FTS reactions.

Fischer-Tropsch synthesis reactions were carried out with a high surface area Fe-Zn-K4-Cu2 catalyst prepared during this reporting period. When compared to the FTS reaction data obtained on the low surface area Fe-Zn-Cu-K samples (Zn/Fe=0.1, K/M=0.02, Cu/M=0.01) studied previously, the high surface area sample exhibited higher CO conversions (38% and 16% respectively at 220^{o}C and a CO space velocity of 5 NL/hr.g-Fe) and CO rates (4.2 and 2 mol/hr.g-at.Fe respectively at 220^{o}C and ~18% CO conversion). The increase in surface area however did not result in significant changes in product selectivities at any of the reaction conditions used. The CO_2 selectivity in both cases were identical, while the CH_4 selectivity was slightly higher on the high surface area sample (2.6% and 1.8% respectively at 220^{o}C, and ~18% CO conversion); and these are likely to be due to a higher surface K/Fe ratio in the high surface area sample.

FTS reactions were also carried out on the high surface area Fe-Zn-Cu-K catalyst at conditions normally used in Co-based FTS reactions (200^{o}C, 20 atm and H_2/CO=2). The H_2/CO ratio was increased on the Fe-Zn-Cu-K sample in order to match the CH_4 selectivity obtained on the Co/SiO_2 catalyst. At this condition (H_2/CO=20), space velocity runs conducted on the Fe-Zn-Cu-K sample showed much lower C_{5+} selectivity (68% compared to 85% for the Co/SiO_2 catalyst). CO_2 selectivities were smaller at higher H_2/CO ratios (6% and 14% respectively at ~16% CO conversion), and independent of CO conversion indicating that secondary water gas

shift reactions do not occur at these high H_2 partial pressures on Fe-Zn-Cu-K. The higher hydrogen surface coverage also leads to a higher termination of chains at lower carbon numbers and hence to a decrease in the product molecular weight. The Fe catalyst also had a higher paraffin content at the higher H_2/CO ratio (*1*-C_6H_{12}/*1*-C_6H_{14} ratio being 0.35 compared to 2.0 at H_2/CO=2, and independent of CO conversion).

Studies on Ru-promotion on a Fe-Zn-K catalyst showed an increase in CO rates and hydrocarbon productivities with an increase in Ru content in the 0-1 at.% range. The primary effect of Ru appears to be in improving dispersion of the Fe_xC structure and hence an increase in the number of available sites for the FTS reaction.

FTS reactions were also carried out with a 21.9 % Co/SiO_2 catalyst at conditions normally used in Fe-based FTS reactions (220°C, 31.6 atm and H_2/CO=2). The H_2/CO ratio was decreased on the Co/SiO_2 sample (to 1.0) in order to approach the CH_4 selectivity obtained on the Fe-Zn-Cu-K catalyst. At these conditions (H_2/CO=1), space velocity runs conducted on the Co/SiO_2 sample showed higher CH_4 selectivities than that of the Fe-Zn-Cu-K catalyst (6% and 2.6% at ~20% CO conversion). The higher CO surface coverage also led to the inhibition of secondary hydrogenation reactions of α-olefins (as shown by the *1*-C_6H_{12}/*1*-C_6H_{14} ratio being unchanged with space time). At this high temperature, secondary chain growth by readsorption of α-olefins is also non-existent as indicated by a fairly linear Flory plot.

During the current reporting period, experiments were also conducted to test the effect of reaction pressure on the performance of a 21.9% Co/SiO_2 catalyst. FTS reactions at 5 atm showed the existence of the water effect even at these conditions. These tests were in preparation for our *in situ* FTIR spectroscopic experiments, which will be conducted to study the autocatalytic water effect on Co catalysts in an infrared reaction cell capable of pressures up to 5 atm.

Task 1. Iron Catalyst Preparation

The objective of this task is to produce robust intermediate- and high-α catalysts.

See Task 2.

Task 2. Catalyst Testing

The objective of this task is to obtain catalyst performance on the catalysts prepared in Task 1.

A. Fischer-Tropsch Synthesis. Comparison of alkali Metals as Promoters

Introduction

The use of alkali promoters has been widely practiced. However, data to compare various promoters is limited for the iron-based catalysts and much of the available data were obtained at low pressure or under a variety of reaction conditions. The importance of the alkali promoter in determining catalytic activity, stability and selectivity merits a comparison of the promoters under suitable reaction conditions. The present study utilizes medium pressure synthesis conditions to compare the alkali promoters under the same reaction conditions and over a wide range of conversion levels.

Experimental

A precipitated iron-silica catalyst base (100Fe:4.6Si atomic ratio) was prepared by continuous precipitation. The calculated quantity of aqueous alkali metal nitrate was added to the dried base material to provide an alkali metal:iron atomic ratio of 100:1.44. As described previously, a 1-L stirred autoclave was used to effect catalyst activation using CO and they subsequent synthesis at 270°C, 1.2 MPa (175 psig), H_2:CO = 0.7, and various space velocities as described previously (same as above). During the course of the run, the conditions were returned

to 3.1 NL/hr/g. Fe, the base flow rate, to obtain data to establish the catalyst deactivation rate and to correct each measured conversion to that of the fresh catalyst.

Results and Discussion

The conversion of CO as a function of the reciprocal of the space velocity shows that the ranking of the alkali metals as a promoter for the activity of an iron catalyst will depend upon the CO conversion level (Figure 1). At low (CO conversion about 20%) the activity of the K and Li promoted catalysts are about the same with the Li promoted catalyst being slightly more active. These two alkali metals are about 2.8 and 2.9 times more active than for Cs and Rb, respectively. However, at 40% CO conversion, potassium is much more active than the other metals with the time required, relative to K, to attain 40% conversion being K:Li:Cs:Rb = 1:2.76:3.24:3.14. As the CO conversion increases to 60% the four metals begin to have a similar impact on activity with K:Li:Cs:Rb = 1:2.15:2.06:1.98. Thus, K is equal to or superior to the other three alkali metals over the entire CO conversion range.

For the selectivity of products by carbon number (alpha value), the four promoters are essentially the same. Thus, while the total activity varies, the distribution of products by carbon number is essentially the same.

The activity for the water-gas-shift (WGS) reaction depends upon the alkali promoter (figure 2). The lower WGS activity will result in a higher partial pressure of water in the exit gas and this is clearly shown in figure 2. The water partial pressure is the highest for the entire range of CO conversions for the catalyst containing the Li promoter. At lower CO conversion levels, K produces the next least effective catalyst for the WGS reaction. Over the lower CO conversion range, Rb and Cs promoters produce a catalyst that is more active than the other two alkali metals; at higher conversion levels the catalysts containing K, Cs and Rb have about the same

water partial pressure. This indicates that using the Li promoter may produce an iron catalyst that more closely resembles cobalt in producing less WGS than the "normal" iron catalyst.

The alkene fraction in the C_2-C_4 olefins also are consistent with Li being different from the other alkali promoters. As the K content of a catalyst is increased, the alkene fraction of the C_2-C_4 products increase and the increase is greatest for the C_2 products. This is the case for the products obtained in the present study. At the lower CO conversion levels, alkenes account for about 85% or more of the C_3-C_4 carbon number products for all four promoters, and there is little difference in the slow decrease in the olefin fraction as the CO conversion increases. However, ethene accounts for only about 55% of the C_2 products with the Li promoter whereas it accounts for 75-80% of the C_2 products with the other three promoters.

References

1. The Fischer-Tropsch and related synthesis, H. H. Storch, N. Golumbic, R. B. Anderson, John Wiley & Son, Inc, New York, 1951, P227

2. R. J. O'Brien, L. Xu, R. - Spicer and B. H. Davis, Energy & Fuels, 10, 921-926 (1996))

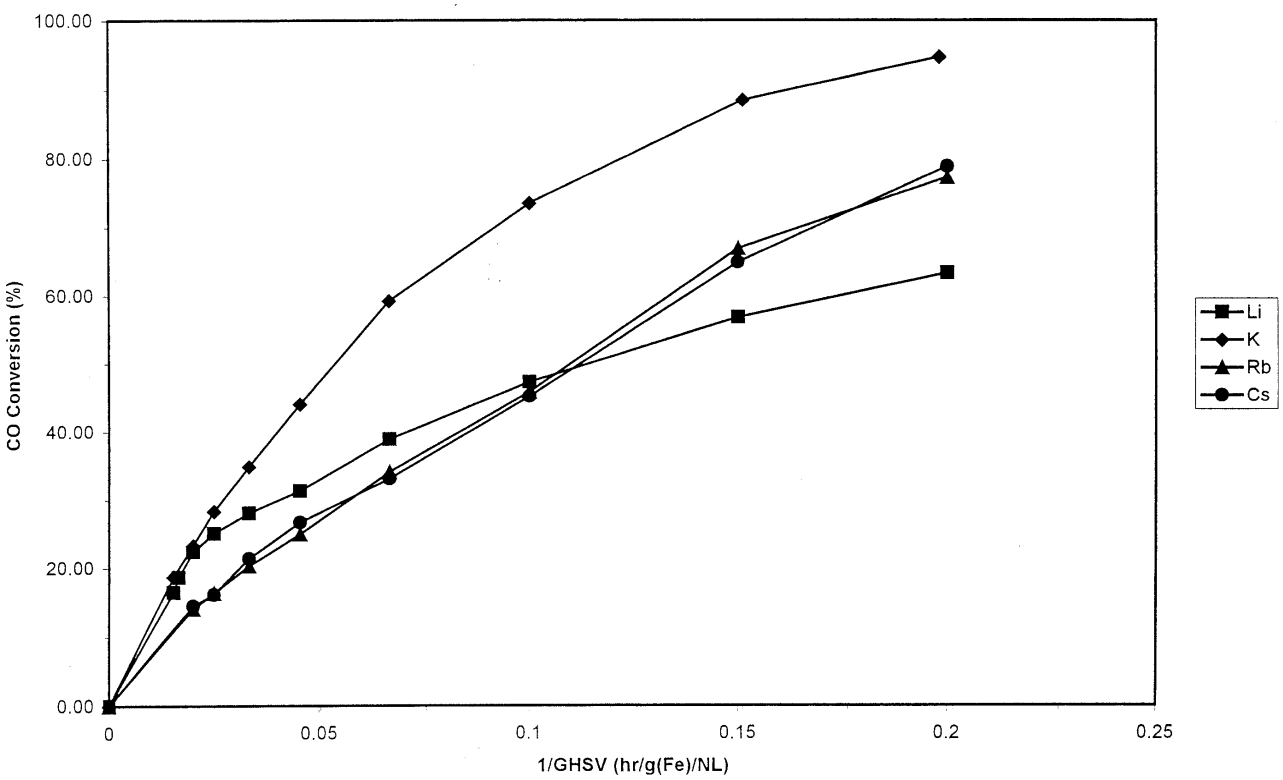

Figure 1. CO conversion corrected as a function of space time, 1.44Li, 1.44K, 1.44Rb, 1.44Cs.

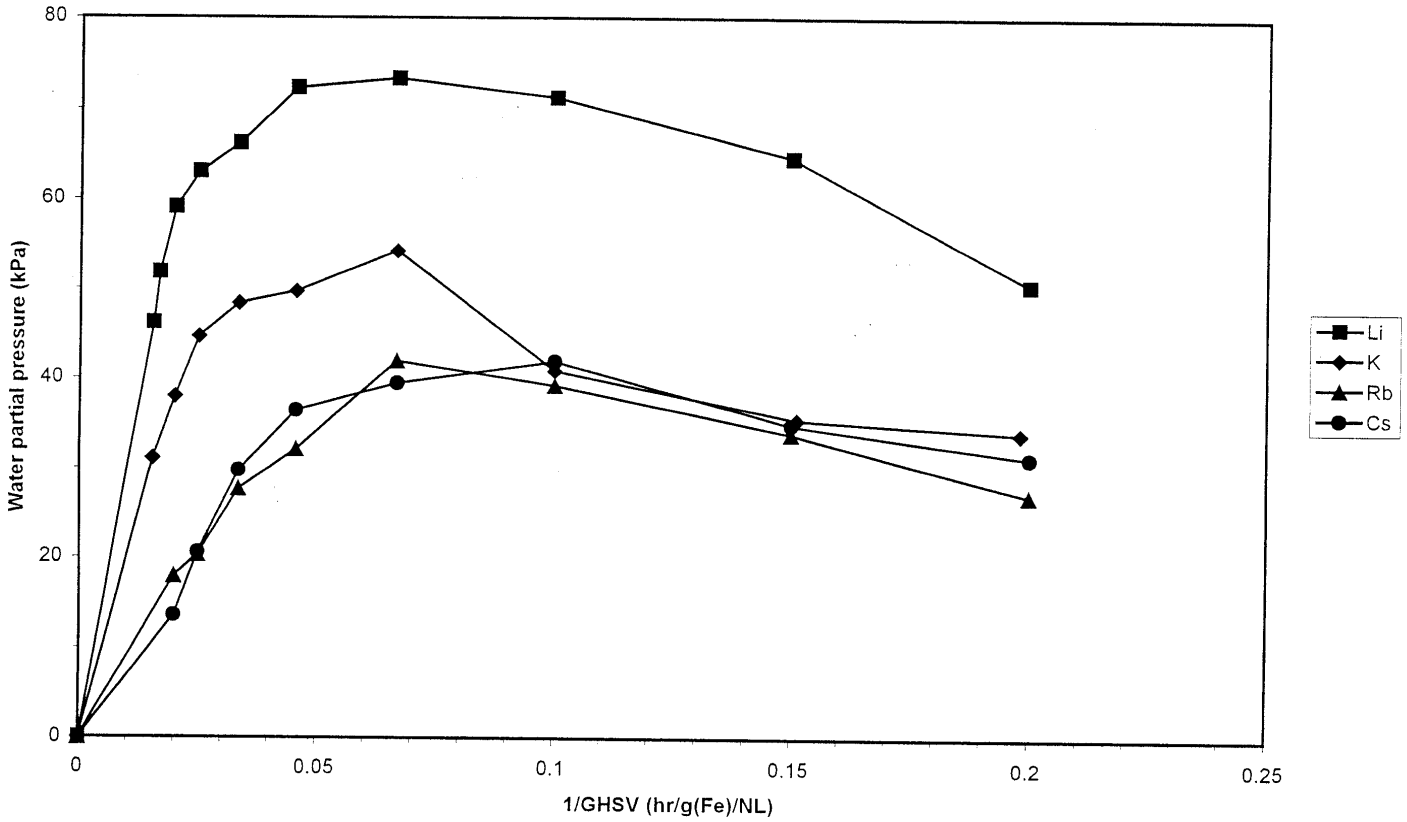

Figure 2. Water partial pressure as a function of space time, 1.44Li, 1.44K, 1.44Rb, 1.44Cs.

Task 3. Catalyst Characterization

The objective of this task is to obtain characterization data of the prepared catalysts using routine and selected techniques.

A. Characterization of Iron Phase Change During Fischer-Tropsch Synthesis Reaction

Introduction

Iron-based Fischer-Tropsch (FT) catalysts undergo a series of phase transformations during activation and use (1). Activation with carbon monoxide or syngas typically results in the conversion of Fe_2O_3 to Fe_3O_4 and ultimately to one or more carbides (2). During FT synthesis, iron carbides can be oxidized to Fe_3O_4 if the H_2O/H_2 or CO_2/CO ratios are high enough (1). There has been considerable debate about the active phase of the FT synthesis. Some studies have indicated an active oxide species (3) while most have supported a carbide species (2,4). Mössbauer spectroscopy has proven to be an effective technique for the analysis of iron-based FT catalysts. *In situ* Mössbauer studies have been reported (5,6); however, these studies have been performed at low pressure and low conversions. Studies performed at industrially relevant conditions have generally involved removing the catalyst from the reactor followed by passivation (7) which, if not performed properly, will oxidize the catalyst (4). Herein are reported the Mössbauer results obtained on an unpromoted precipitated iron catalyst that was activated and reacted in a slurry phase, continuous stirred tank reactor at high conversion and under industrially relevant conditions. Strict measures were observed to prevent oxidation of the catalyst samples. The Fe-Si, Fe-K, Fe-Si-K catalysts were all studied using the same methods.

Experimental

Catalysts were prepared by a previously described procedure (2). A slurry of 64.4 g of catalyst (32.2 g Fe) and 290 g of Ethylflo 164 decene trimer was charged into a one liter

autoclave operated as a continuous stirred tank reactor. The catalyst was activated with carbon monoxide (2 L h^{-1} g·Fe^{-1}, STP) at 270^{O}C and 1.3 MPa for 24 hours. Following activation, syngas flow was initiated (3.1 L h^{-1} g·Fe^{-1}, STP) and the temperature and pressure were maintained. Catalyst slurry samples (5-10 g) were removed from the reactor under an argon atmosphere via a dipleg immediately after activation and at various times during FT synthesis. Light wax was extracted from the cooled slurry samples under an argon atmosphere with deoxygenated tetrahydrofuran. Catalyst samples were loaded into sealed plexiglass holders for analysis by Mössbauer spectroscopy. The spectra were collected by a conventional constant acceleration spectrometer using a 30 mCi ^{57}Co in rhodium matrix.

Results

Syngas conversion versus time on stream for unpromoted iron catalyst is shown in Figure 1. Syngas conversion after 24 hours of FT synthesis was above 84%. Catalyst activity declined steadily throughout the run with an average rate of deactivation of 0.16 % h^{-1} (absolute syngas conversion).

Catalyst samples for Mössbauer spectroscopy were withdrawn immediately after activation and at 23 h, 168 h and 453 h of FT synthesis. The distribution of iron in the catalyst after activation with carbon monoxide was 94 % χ-Fe_5C_2 and 6 % Fe_3O_4. Exposure to syngas initiated oxidation of the χ-Fe_5C_2 to Fe_3O_4. After 23 hours of FT synthesis, 83 % of the iron was present as χ-Fe_5C_2 and the balance was Fe_3O_4. The amount of iron present as χ-Fe_5C_2 had decreased to 18 % after 168 hours of FT synthesis. The only detectable phase after 453 hours of FT synthesis was Fe_3O_4.

The deactivation rates of Fe-Si, Fe-K, and Fe-K-Si have been determined and the catalyst samples have been withdrawn from the reactor right after activation and at different conversion

levels. The Mössbauer spectra of the catalysts are going to be recorded to identify the phase changes.

The Fischer-Tropsch synthesis activity of unpromoted, potassium promoted (100Fe/0.71K), silica promoted (100Fe/4.6Si) and double promoted (100Fe/4.6Si/0.71K) catalysts were plotted in Figure 2. It can been seen from Figure 2 that Fe and Fe-K catalysts have essentially the same activity during the initial induction period (within 50hrs time on stream) which is higher than Fe-Si and Fe-Si-K catalysts. But the activity of both Fe and Fe-K catalyst decrease steadily with time on stream. For Fe-Si and Fe-Si-K catalysts, they both undergoes an induction period, the activity first goes up until it reaches the maximum and then decrease slowly. After 94 hours of synthesis, the CO conversion of Fe-Si catalyst was 76.1% while the Fe-Si-K catalyst reaches its maximum conversion of 84.04% at 163 hrs time on stream. The average deactivation rate for the catalysts are Fe-K(48%/week), Fe(41%/week), Fe-Si(39%/week) and Fe-Si-K(33%).

Discussion

Based on data generated from several catalysts, a model of the working FT catalyst was developed. In this model, the initial catalyst was essentially comprised of a mixture of iron carbides. As the reaction progressed, the carbide fraction decreased to attain a value of about 30-40%. During this phase change, the conversion did not decrease appreciably. To account for the nearly constant activity while the phase changed a model was proposed. This model had the assumption that the core of each particle was oxidized to form Fe_3O_4 and an out layer remained a carbide form; thus, the surface of the catalyst remained essentially the carbide form while the ratio of oxide/carbide increased as the core consisting of Fe_3O_4 expanded to approach a “steady state at carbide/oxide ratio.

The results with the unpromoted catalyst do not agree with this model. Instead, it appears that the catalyst particle converts from the carbide to the oxide form in parallel with the decline in conversion. Thus, it appears that a steady-state surface carbide phase/core Fe_3O_4 phase is not formed for the unpromoted iron catalyst. One explanation to account for this is that the rate of carbide oxidation is dependent upon the particle size for the unpromoted catalyst. Work underway with single and doubly promoted catalysts should allow us to define the role of each promoter in determining the composition of the working catalysts.

References

1. Dry, M. E. In Catalysis-Science and Technology; Anderson, J. R., Boudart, M. Eds.; Springer-Verlag: New York, 1981; Vol. 1, pp 196-198.
2. O'Brien, R. J., Xu, L., Spicer, R. L., Davis, B. H., Energy & Fuels, 10, 921 (1996).
3. Reymond, J. P., Mériaudeau, P., Teichner, S. J., J. Catal., 75, 39 (1982).
4. Shroff, M. D., Kalakkad, D. S., Coulter, K. E., Köhler, S. D., Harrington, M. S., Jackson, N. B., Sault, A. G., Datye, A., J. Catal., 156, 185 (1995).
5. Berry, F. J., Smith, M. R., J. Chem. Soc. Faraday Trans., 85, 467 (1989).
6. Raupp, G. B., Delgass, W. N., J. Catal., 58, 361, (1979).
7. Huang, C. S., Ganguly, B., Huffman, G. P., Huggins, F. E., Davis, B. H., Fuel Sci. Technol. Int., 11, 1289 (1993).

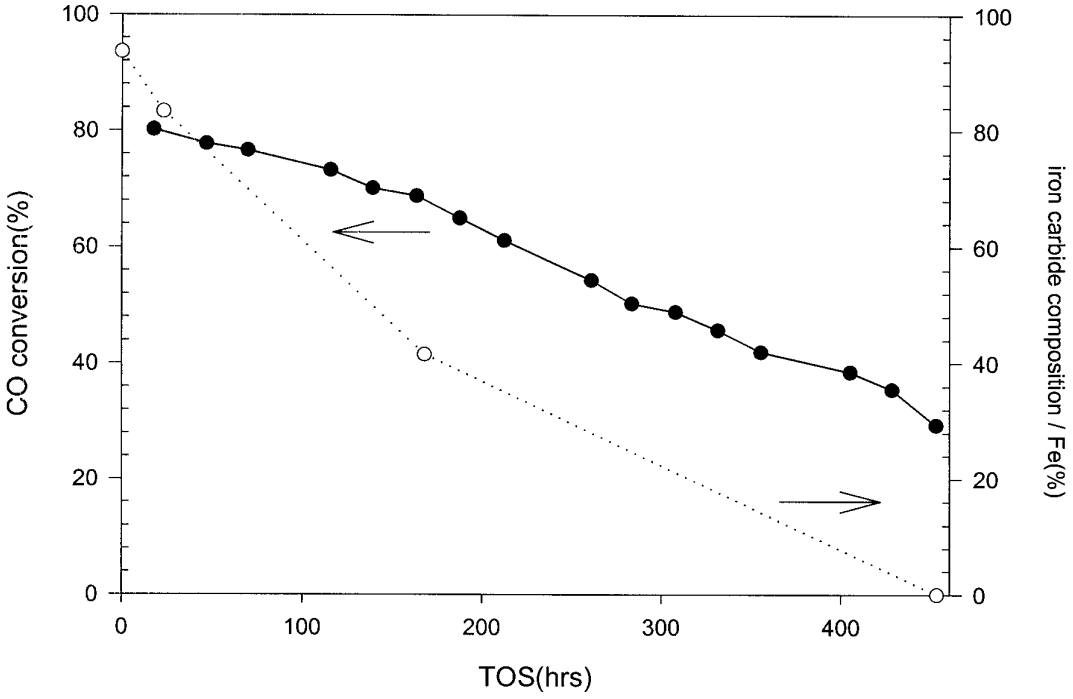

Figure 1. Catalytic activity and iron carbide percentage versus reaction time.

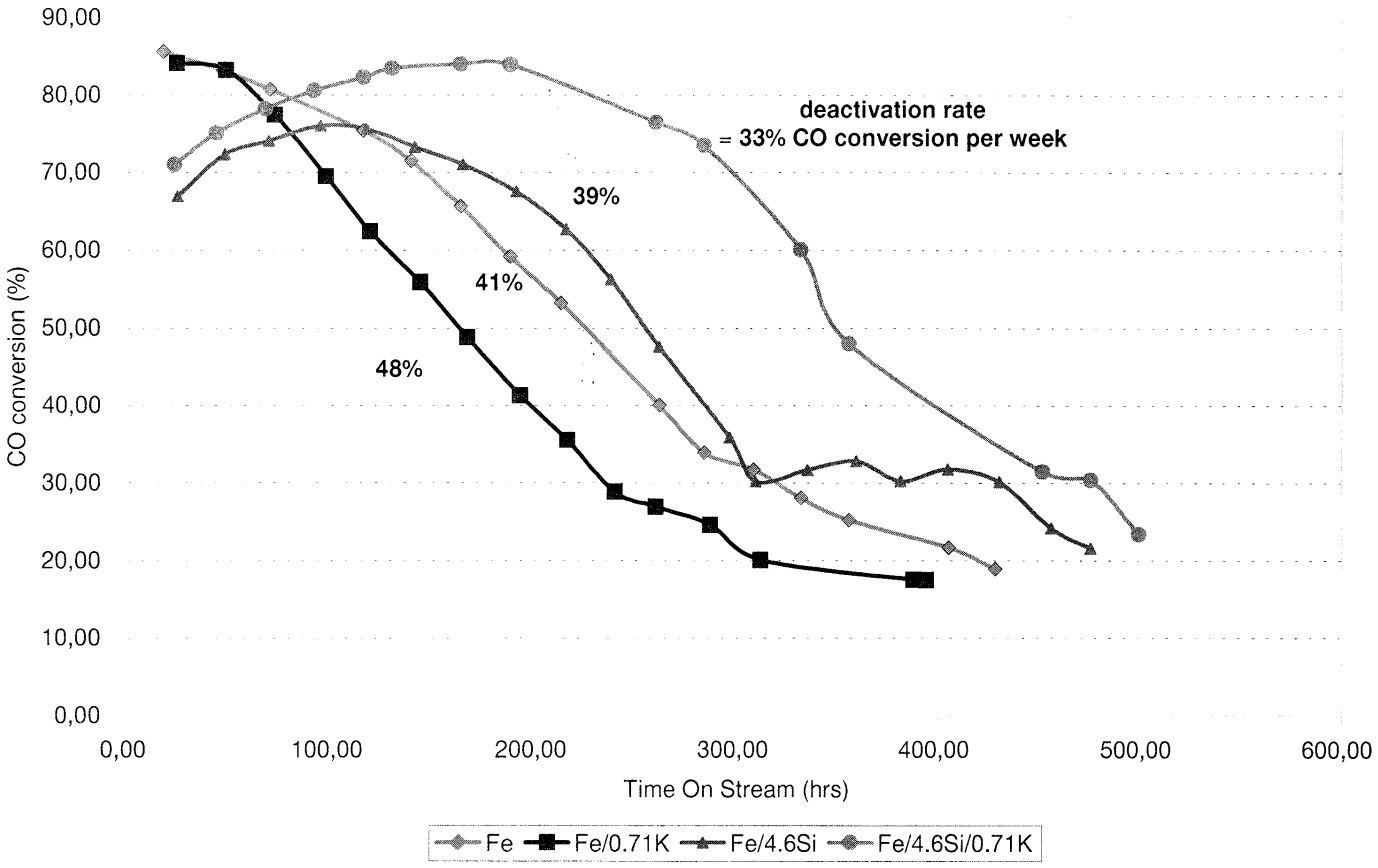

Figure 2. CO conversion as a function of time-on-stream.

B. Characterization of promoted Cobalt FTS Catalysts

Introduction

We have studied and are continuing to study the impact on reducibility of cobalt by the use of different supports and by the incorporation of different promoters and additives to supported cobalt catalysts. Although the use of different supports and promoters is well documented, what is less well understood are the reasons for the differences in deactivation rates of these catalysts. Only by rigorous characterization can the properties of the catalysts brought about by differences in preparation, support, and degree and type of promoter be linked to the resulting catalytic properties under reaction. We therefore have spent considerable attention on the characterization of not only the fresh catalysts, but also the spent catalysts sampled after many days on stream in the continuously stirred tank reactor. With this approach, it is our goal to understand what properties are required for high initial activity and, just as importantly, for the maintaining of high stability, and how to achieve them in the catalyst preparation and activation steps. Interestingly, while addition of promoters can markedly improve the reducibility of cobalt FTS catalysts, leading to more available catalytic sites for reaction, these catalysts often display significantly high rates of deactivation. This raises many questions, which should be able to be addressed through careful characterization. For example, is the reducibility of the metal sites changing under reaction conditions and if so, what are the reasons? Is the cobalt and/or promoter cluster size changing under reaction or is there loss in the degree of interaction between the two? Are we forming mobile metal carbonyl species by the addition of CO that leads to loss of metallic sites and changes in the morphology of the clusters with time onstream? To address these questions, we are employing several characterization techniques, including temperature programmed reduction (TPR), hydrogen chemisorption, X-ray diffraction (XRD), transmission

electron microscopy (TEM), and in the near future, diffuse reflectance infrared Fourier transform spectroscopy (DRIFTS) and X-ray absorption spectroscopy methods (XAS) such as extended X-ray absorption fine structure (EXAFS) and X-ray absorption near edge structure (XANES).

Experimental

BET Surface Area Measurements

BET measurements for all catalysts were conducted to determine the loss of BET surface area with loading. These experiments were conducted using a Micromeritics Tri-Star system. Prior to testing, samples were slowly ramped to 160°C and evacuated for 4hrs to approximately 50mTorr.

Hydrogen Chemisorption by the Temperature Programmed Desorption (TPD) Method

Hydrogen chemisorption was measured using a Zeton Altamira AMI-200 unit which incorporates a thermal conductivity detector (TCD). Catalysts were activated using pure hydrogen at the desired reduction temperature (usually 300 or 350°C) for 10hrs and cooled under flowing hydrogen to 100°C. The sample was held at that temperature under flowing argon to remove physisorbed and weakly bound species, prior to increasing the temperature slowly to the activation temperature. At that temperature, the catalyst was held under flowing argon to desorb remaining chemisorbed hydrogen until the TCD signal returned to the baseline. The TPD spectra was integrated and the amount of desorbed hydrogen determined by comparing to the areas of calibrated hydrogen pulses. Table 2 shows the resulting dispersion based on total weight of metal in the sample for a number of cobalt FTS catalysts.

X-ray Diffraction

Diffraction patterns were recorded using a Rigaku X-ray diffractometer utilizing CuK_{Alpha} radiation. Because quantitative information was desired on particle size, we scanned the

oxidized samples for the peak corresponding to the (311) planes of Co_3O_4, which appears at a 2θ value of approximately 37. Scans were taken using a step size of 0.010°. Because of the level of noise for small cobalt clusters, each point was scanned for 10 seconds to improve resolution. Two different software packages were used to fit the results, Jade and Winfit. Peak position and size values for both software packages are included in Table 2.

Transmission Electron Microscopy

Transmission electron microscopy (TEM) imaging was conducted using a JEOL2000FX, which incorporates a 200keV LaB_6 gun. Samples were first reduced in hydrogen at 350°C for 10hrs in a 2:1 Ar:H_2 mixture (as performed prior to catalytic activity testing) and passivated using 1%O_2 in helium passivation gas. Next, they were passed through a 75 micron sieve, and suspended in isopropyl alchohol, prior to loading onto the Lacey carbon on Cu grid, and subsequent drying. Imaging was conducted at various magnifications including 50, 100, 250 and 400K. Negatives and prints were developed, and clusters counted with size to obtain a distribution, where possible. Figures 1 a and b show a TEM micrograph and resulting particle size distribution for a fresh 0.5% Re promoted 15%Co/Al_2O_3 catalyst, while Figures 2 a and b display results for a spent 0.2% Re promoted 15%Co/Al_2O_3 catalyst sampled after reaching a steady state conversion in the CSTR.

Temperature Programmed Reduction

Temperature programmed reduction (TPR) profiles of fresh and spent catalysts were also recorded using the Zeton Altamira AMI-200 unit. Calcined fresh samples were first purged in flowing inert gas to remove traces of water. Spent catalysts were either removed from the reactor via a dip tube during the run, or sampled after completion of a run. In each case, the catalyst sampled reflected the steady state condition of the run. The wax was first extracted using

xylenes in a Soxhlet apparatus and the catalyst collected in a 33mm×80mm extraction thimble. The catalyst was dried in an oven at 110°C and then reoxidized under flowing dry air after ramping to 250°C before TPR was conducted. TPR was performed using a 10%H_2/Ar mixture and referenced to Ar. Resulting profiles were normalized to the height of the main peak so that shifts in the peak positions could be ascertained.

Results and Discussion

BET Surface Area Measurements

Table 1 displays the BET surface area results. The 15%Co catalysts loaded onto Condea Vista B Al_2O_3 had an average BET surface area of 157 m^2/g. The Davisil SiO_2 supported catalysts had higher BET surface areas, with the 15% loaded catalysts on Davisil 644 SiO_2 support averaging 208 m^2/g and the 15% loaded catalysts on Davisil 952 SiO2 support averaging 229 m^2/g. The 20% loaded catalysts on Davisil 952 SiO_2 support modified by ZrO_2 had a lower average BET area of 197 m^2/g. Not surprisingly, the series of catalysts supported on Davisil 952 (ZYQ028 through ZYQ032) exhibited decreasing surface areas with increasing Co loading. Each 5% increase in loading yielded drops in BET surface area in the order 260, 234, 226, 190, and 170 m^2/g, respectively. The 15% Co catalysts prepared on Shell 980F had an average BET surface area of 103 m^2/g, while the one prepared on Shell 980G was much lower at 52.3 m^2/g. The 15% cobalt catalyst on Dagussa P25 TiO_2 had the lowest BET surface area of 41.8 m^2/g.

H_2 Chemisorption, XRD and TEM

Dispersion calculations were based on the assumption that the H:Co stoichiometric ratio was 1:1. In general, particle size estimates from H_2 chemisorption measurements are based on the assumption that the metal clusters are completely reduced. One determines the total number of atoms from knowledge of the weight % of loading of the metal and the surface atoms from the

desorption of hydrogen. By assuming a particular geometry (e.g., a spherical or cubic structure), one is able to deduce the average cluster size. However, in our case, the assumption of complete reduction may or may not be valid, depending on the support used and type and degree of promotion. TPR results provide a general indicator for the extent of reduction. In the case where metal oxide clusters remain on the surface during chemisorption (incomplete reduction), the cluster size determination will overestimate the cluster size. This may be particularly important for unpromoted catalysts supported on TiO_2 and Al_2O_3, where significant metal-support effects occur. For these samples, a considerable fraction of clusters is reduced at very high temperatures in the TPR profiles. For example, assuming complete reduction for 15%Co/Al_2O_3 leads to a value of 64 nm for the average cluster size. XRD clearly reveals, however, that the cluster is no different in size from the promoted catalysts, however, which are accurately predicted by H_2 chemisorption measurements. Despite the problem with cluster size approximation, the calculated dispersion based on hydrogen uptake should provide an accurate indicator of the number of surface atoms available for reaction, and these can be used appropriately for determining turnover numbers in catalytic testing.

Reaction testing in CSTRs has been conducted primarily on promoted 15%Co/Al_2O_3 catalysts (ZYQ036, 039, 040, and 041). These catalysts displayed the highest uptakes of H_2, significantly higher than that of the unpromoted catalyst (ZYQ000). Assuming complete reduction of the Co in the case of the promoted catalysts, the clusters for fresh catalysts were determined to be approximately 12 nm, 14 nm, 12 nm, and 11 nm for 0.5%Pt-15%Co/Al_2O_3, 0.2%Re-15%Co/Al_2O_3, 0.5%Re-15%Co/Al_2O_3, and 1%Re-15%Co/Al_2O_3 catalysts, respectively. These values are in reasonably good agreement with the values determined by XRD and TEM. For the 0.5%Re-15%Co/Al_2O_3 catalyst, the metal clusters were found to be primarily

approximately 10 nm. For the case of XRD, to convert to the metallic particle size, the multiplier 0.75 should be used. Therefore, it appears that the XRD fitting software Jade fits the results more closely to the actual value, while Winfit apparently underestimates the cluster size.

Characterization of the spent samples was also attempted, and values are reported in parentheses. Further testing is currently being conducted to verify the validity of the results. For example, in hydrogen chemisorption, clusters must be cleaned sufficiently of wax before accurate TPD measurements are obtained. Due to time constraints, in XRD, we only scanned the range where the Co_3O_4 (311) peak occurred at a 2θ of 37. However, further tests are necessary to determine if any other species are present. For example, cobalt rhenium oxide may form after reoxidation for the case of the Re promoted catalysts. Interestingly, a new peak formed at 2θ = 38.5 for spent catalysts, and often dominated in intensity over the peak positioned at 2θ = 37. We are currently investigating the nature of this new peak, which did not appear in the case of the fresh catalysts.

Temperature Programmed Reduction

Figure 3 shows the TPR profiles for the unpromoted cobalt catalysts. For the two SiO_2 supported catalysts, two peaks emerged, attributed to the reduction of Co_3O_4 to CoO, which decomposes at higher reduction temperatures to metallic Co. As shown in the figure, the addition of surface ZrO_2 to silica did not significantly change the reducibility. In addition to the two peaks observed for the Co/SiO_2 catalysts, the TiO_2 and Al_2O_3 supported cobalt catalysts displayed broad peaks at higher temperatures, due to the metal support interaction, which increases with decreasing cluster size. For the Co/Al_2O_3 catalyst, an additional low temperature peak is observed, which we assign to the reduction of cobalt nitrate species. Calcining the

catalyst at higher temperatures removed this low temperature (200°C) peak.. Therefore, the decomposition of Co precursors was concluded to be more difficult on Al_2O_3 support.

Figure 4 shows a TPR comparison of noble metal promoted catalysts prepared using a variety of supports. The addition of Pt or Ru to the support had a similar effect on each of the supported catalysts. All the peaks shifted markedly to lower temperatures, presumably due to spillover of H_2 from the reduced promoter to reduce Co oxide species. Of particular importance, peaks attributed to the metal support interaction for Co species on TiO_2 and Al_2O_3 are reduced at much lower temperatures, freeing up the availability of metal atoms for reaction. For the case of Re, the reduction of Re occurs at higher temperatures than Pt or Ru. This is clearly shown in Figure 4. Although the low temperature peaks are not significantly affected, Re still plays a valuable role in reducing the reduction temperature of species for which there is a significant metal-support interaction.

Figures 5 through 12 show the effect of increasing promoter or additive loadings on the reduction temperature for different supported cobalt catalysts. Figure 5 reports the addition of Ru to the 15%Co/SiO_2 catalysts. With the addition of 0.2% Ru, the greatest shift was found to be that of the low temperature peak which we ascribed to the reduction of Co_3O_4 to CoO. The position of the higher temperature peak assigned to further reduction of CoO to metallic increased slightly. However, further increases in promoter shifted both peaks to lower temperatures. Interestingly, further addition of Ru beyond 1% loading led to only marginal further decrease in temperature.

For the Pt series, the same atomic ratios were used as with Ru, so higher weight percentages of Pt were used. Increasing the Pt loading, in general, led to expected decreases in the reduction temperature, and lower temperatures were achieved on a molar basis with Pt

relative to Ru. One exception to the trend was the 0.97% loaded catalyst. Catalysts will be tested in the future by ICP to verify weight percentages.

Figure 7 demonstrates the impact of modifying the surface of SiO_2 with ZrO_2 and incorporating noble metal promoters. As with the SiO_2 catalysts, a large shift was observed for the low temperature peak when Ru or Pt was added, while only a modest shift to lower reduction temperatures was observed for the higher temperature peak. Interestingly, the Re promoted catalyst behaved much differently, where both peaks shifted slightly to higher temperatures. This suggests that reduction of Re occurs at much higher temperatures than the Pt or Ru catalysts.

Examination of Figure 8 reveals an interesting result when the K concentration is increased for the 15%Co/SiO_2 support. Addition of a small amount (0.5%K) to the catalyst resulted in a remarkable shift to lower temperatures for both peaks (160°C for the low temperature peak and 60°C for the high temperature peak). However, further increases in the K content shifted both peaks back up to higher temperatures, beyond the peak positions of the unpromoted reference catalyst.

Figures 9 through 12 focus on promoting Al_2O_3 support. Unlike the SiO_2 supported cobalt catalysts, there is a strong interaction of the cobalt with the support for a large fraction of the cobalt clusters. Again, evidence for this effect is demonstrated by the broad peak at high temperatures in the TPR profile for the unpromoted catalyst. Therefore, the potential for achieving gains in activity by promoting the support are high.

Figures 9 and 10 show profiles for Re promoted 15%Co/Al_2O_3 catalysts. The difference between the two series of catalysts is in the preparation. The series in Figure 9 references catalysts ZYQ039, 040 and 041, which were prepared by loading the Co three times by successive incipient wetness impregnation steps, where the catalyst was dried between each step.

Only one calcination was used after the last step. Figure 10 references catalysts ZYQ051, 052, and 052. These catalysts were prepared in a similar manner, except that the each of the catalysts was calcined after each sequential impregnation and drying step, for a total of three times. Comparing Figure 10 to Figure 9 reveals that no benefit to reducibility was achieved by calcining the catalyst sequentially.

Figure 9 shows that with each increase in loading of Re promoter, the low temperature peak did not change. Again, we ascribe this to the higher reduction temperature of Re in comparison with the Ru and Pt promoters. Interestingly, however, the high temperature peak shifts markedly with each increase in the Re loading. Therefore, we conclude that after reduction temperature of Re is reached, then spillover of H_2 occurs to lower the reduction temperature of Co oxide species for which there is a significant interaction with the support.

As described earlier, both Pt and Ru promoters behave in a similar manner and shift both reduction peaks to lower temperatures for 15%Co/Al_2O_3. Figure 11 demonstrates that by increasing the loading of Ru, both reduction peaks shift to lower temperatures, with the effect being more pronounced for the low temperature peak. Remarkably, when a loading of 0.5% Ru is achieved, the broad high temperature peak ascribed to the interaction of the support with the metal has shifted by approximately 100°C. Unfortunately, further increases in loading, and in fact doubling the loading, shows only a marginal improvement in reducibility. Two additional catalysts were prepared incorporating La and Zr to the catalysts. However, no change in the low temperature peak was observed.

Metal-support effects were also seen for the 10%Co/TiO_2 catalysts. Therefore, the potential benefits for increasing available metal atoms for reaction by promoting the catalyst were high. A number of different promoted catalysts were tested by TPR, and results are

depicted in Figure 13. While addition of B to the catalyst had adverse effects on reducibility, the noble metals had an enhancing effect. In a similar manner with Al_2O_3, both Pt and Ru shifted all peaks in the TPR profiles to lower temperatures, while Re only benefitted the high temperature peaks.

Although promoted catalysts displayed a higher initial activity as expected, due to increased availability of metal atoms for reaction, the deactivation rates differed greatly. In an effort to further understand the differences in deactivation patterns of promoted supported Co catalysts, we have begun to characterize the spent samples, either removed during the run by a dip tube or after the run. In each case, the catalyst was removed after a steady state conversion was achieved. Again, catalysts was sampled, the wax was removed first by extraction with xylenes in a Soxhlet apparatus, and the catalyst was oxidized in flowing dry air at 250°C.

We wished to determine if significant differences in reducibility occurred by comparing TPR profiles for the spent catalysts in reference to the fresh catalyst. We hypothesized that one route to deactivation might be if the promoter-cobalt interaction was decreased due to segregation, agglomeration, or removal by the leaching out of one or both metals as a mobile species (e.g., a metal-carbonyl). If the reducibility changed, then the TPR for the spent would become more like the TPR profile of the unpromoted catalyst. Therefore, in Figures 15 through 18, we have displayed TPR spectra of the fresh, spent, and unpromoted catalysts such that qualitative comparisons could be ascertained.

Before examining the TPR profiles of the promoted catalysts, it is instructive to first review the TPR profiles of the fresh and spent unpromoted catalysts (see Figure 14). Interestingly, both peaks shift to higher reduction temperatures, and the high temperature peak for the spent catalyst is significantly sharpened. This raises questions as to the reducibility of the

Co with changes in the cluster size. XRD results indicate a decrease in cluster size for the unpromoted catalyst. One might conclude that a smaller cluster would lead to an increase in the interaction between the support and the cobalt and a shift to higher reduction temperatures in the TPR spectra.

Although Pt promotion gave the largest shifts in reduction temperature for the fresh catalysts, in comparison with other promoted catalysts such as Re and Ru, a 0.53% promoted 14.3%Co catalyst displayed a very high rate of deactivation under FTS reaction. Comparison of the TPR for the spent catalyst in reference to the fresh catalyst showed a strong shift to higher reduction temperatures. There is a strong possibility, therefore, that the metal-promoter surface interface decreases under reaction conditions. Future EXAFS investigations may reveal these changes, as EXAFS is one of the most powerful techniques available for determining local structure surrounding the atom of interest. The TPR spectra for the spent catalyst looks much more like the spectra of the unpromoted catalyst than that of the fresh.

Interesting the comparisons for Re and Ru display a much different result. For these catalysts, the reduction peaks appear near or below the peaks observed for the fresh catalysts, indicating that the metal-promoter interaction remains intact under reaction. Interestingly, these catalysts displayed lower rates of deactivation in comparison with the Pt. The peaks of the Re catalysts also were found to be sharper for the case of the spent catalysts. Again, future EXAFS, XRD, and H_2 chemisorption experiments may reveal the reason for the sharpening.

Conclusions

The activity of cobalt catalysts is generally ascribed to the active sites located on the surface of cobalt metal clusters formed after reduction of the oxidic species formed after calcination. However, the reducibility of cobalt catalysts is strongly influenced by the nature of

the support and the degree of promotion by additives, which is the focus of this work. In general, a tradeoff exists as one increases the reduction temperature to activate the cobalt catalyst. Although more sites are reduced, cobalt clusters sinter at higher reduction temperatures. Therefore, TPR and hydrogen chemisorption studies should be conducted prior to catalytic testing, in order to determine the appropriate temperature for catalyst activation. In general, the number of active sites available after reduction varies with support, promoter type, and degree of promotion. The reason for deactivation of promoted FTS catalysts is a subject requiring further study. TPR studies suggest that there is a difference in the degree of interaction of the promoter with the cobalt after reaction testing for each promoter. However, further experiments, using such techniques as EXAFS, are necessary to determine the extent of these morphological changes. Not only will EXAFS allow the determination of cluster size, but the local structure surrounding Co, including the promoter interaction, may be quantified for the fresh and spent catalysts.

The addition of Pt or Ru to the support had a similar effect on each of the fresh supported catalysts. All the reduction peak positions shifted markedly to lower temperatures, due to spillover of H_2 from the reduced promoter to reduce Co oxide species. Of particular importance, peaks attributed to the metal support interaction for Co species on TiO_2 and Al_2O_3 are reduced at much lower temperatures, freeing up the availability of metal sites for reaction. For the case of Re, the reduction of Re occurs at higher temperatures than Pt or Ru. Although the low temperature peaks are not significantly affected, Re still plays a valuable role in reducing the reduction temperature of species for which there is a significant metal-support interaction.

TPR analysis of spent promoted 15%Co/Al_2O_3 catalysts revealed that while observed peaks for Ru and Re promoted catalysts remained shifted to low temperatures, the peaks had

shifted substantially to higher temperatures in the case of the Pt catalyst. This suggests that the Co and Pt interaction is rapidly lost under reaction, and may be the reason for the higher observed deactivation rate.

Table 1

Catalyst Characteristics

Sample ID	Sample Composition	Calcination	BET SA (m_2/g)	+/-	Avg. Pore (nm)	Additional Comments
ZYQ000	15%Co/Al_2O_3	400ºC, flow, 1X	157.7	0.2	4.2	IWI (3X); Condea Vista B, 100-200 mesh
ZYQ001	15%Co/SiO_2	400ºC, no flow, 1X	217.1	0.7	7.7	IWI (3X); Davisil 644 SiO_2
ZYQ002	0.2%Ru-15%Co/SiO_2	400ºC, no flow, 1X	222.0	0.6	7.7	IWI (3X); Davisil 644 SiO_2
ZYQ003	0.5%Ru-15%Co/SiO_2	400ºC, no flow, 1X	233.6	0.5	7.4	IWI (3X); Davisil 644 SiO_2
ZYQ004	1.0%Ru-15%Co/SiO_2	400ºC, no flow, 1X	205.6	0.6	7.6	IWI (3X); Davisil 644 SiO_2
ZYQ005	2.0%Ru-15%Co/SiO_2	400ºC, no flow, 1X	208.9	0.5	7.6	IWI (3X); Davisil 644 SiO_2
ZYQ006	0.39%Pt-15%Co/SiO_2	400ºC, no flow, 1X	200.7	0.6	7.7	IWI (3X); Davisil 644 SiO_2
ZYQ007	0.97%Pt-15%Co/SiO_2	400ºC, no flow, 1X	224.2	0.7	7.6	IWI (3X); Davisil 644 SiO_2
ZYQ008	1.93%Pt-15%Co/SiO_2	400ºC, no flow, 1X	169.6	0.5	4.4	IWI (3X); Davisil 644 SiO_2
ZYQ009	3.86%Pt-15%Co/SiO_2	400ºC, no flow, 1X	217.0	0.6	7.3	IWI (3X); Davisil 644 SiO_2
ZYQ010	0.5%K-15%Co/SiO_2	400ºC, no flow, 1X	210.9	0.5	7.9	IWI (3X); Davisil 644 SiO_2
ZYQ011	1.5%K-15%Co/SiO_2	400ºC, no flow, 1X	200.8	0.5	8.1	IWI (3X); Davisil 644 SiO_2
ZYQ012	3.0%K-15%Co/SiO_2	400ºC, no flow, 1X	168.6	0.4	8.9	IWI (3X); Davisil 644 SiO_2
ZYQ013	5.0%K-15%Co/SiO_2	400ºC, no flow, 1X	214.0	0.6	7.5	IWI (3X); Davisil 644 SiO_2
ZYQ014	15%Co/SiO_2	400ºC, flow, 1X	223.9	0.6	7.5	IWI (3X); Davisil 644 SiO_2
ZYQ015	15%Co/SiO_2	400ºC, flow, 1X	100.0	0.4	15.0	Excess H_2O Impreg (2X); Shell SiO_2 980F, 500 µm
ZYQ016	15%Co/SiO_2	400ºC, flow, 1X	103.4	0.4	15.2	Excess H_2O Impreg (1X); Shell SiO_2 980F, 500 µm
ZYQ017	15%Co/SiO_2	400ºC, no flow, 1X	84.7	0.3	17.3	Excess H_2O Impreg (2X); Shell SiO_2 980F, 500 µm
ZYQ018	15%Co/SiO_2	400ºC, flow, 1X	112.3	0.3	14.8	Excess H_2O Impreg (2X); Shell SiO_2 980F, 250 µm

Sample ID	Sample Composition	Calcination	BET SA (m_2/g)	+/-	Avg. Pore (nm)	Additional Comments
ZYQ019	15%Co/SiO_2	400ºC, flow, 1X	114.2	0.4	15.3	Excess H_2O Impreg (2X); Shell SiO_2 980F, 150 µm
ZYQ020	15%Co/SiO_2	400ºC, flow, 1X	105.5	0.4	15.8	Excess H_2O Impreg (2X); Shell SiO_2 980F, 50 µm
ZYQ021	15%Co/SiO_2	400ºC, flow, 1X	52.3	0.2	10.9	IWI (3X); S 980G 2.3, 60-200 mesh
ZYQ022	15%Co/Al_2O_3	400ºC, flow, 1X	171.3	0.7	2.0	IWI (3X); Condea Vista B, 100-200 mesh
ZYQ023	15%Co/SiO_2	400ºC, flow, 1X	231.9	0.8	7.2	IWI (3X); Davisil 952 SiO_2
ZYQ024	15%Co/TiO_2	400ºC, flow, 1X	41.8	0.2	12.3	IWI (3X); Degussa TiO_2 (P25), 100-200 mesh
ZYQ025	15%Co/SiO_2	400ºC, flow, interval 3X	226.0	0.7	9.1	IWI (3X); Davisil 952 SiO_2
ZYQ026	15%Co/SiO_2	400ºC, flow, 1X	229.3	0.5	7.3	IWI (3X); Davisil 644 SiO_2
ZYQ027	15%Co/SiO_2	400ºC, flow, 1X	240.1	0.7	9.3	Excess H_2O Impreg (2X); Davisil 952 SiO_2
ZYQ028	5%Co/SiO_2	400ºC, no flow, 1X	259.7	1.0	10.0	IWI (1X); Davisil 952 SiO_2, 60-80 mesh
ZYQ029	10%Co/SiO_2	400ºC, no flow, 1X	234.1	0.9	9.8	IWI (2X); Davisil 952 SiO_2, 60-80 mesh
ZYQ030	15%Co/SiO_2	400ºC, no flow, 1X	226.3	0.7	9.6	IWI (3X); Davisil 952 SiO_2, 60-80 mesh
ZYQ031	20%Co/SiO_2	400ºC, no flow, 1X	190.0	0.5	9.0	IWI (4X); Davisil 952 SiO_2, 60-80 mesh
ZYQ032	25%Co/SiO_2	400ºC, no flow, 1X	170.0	0.6	7.8	IWI (5X); Davisil 952 SiO_2, 60-80 mesh
ZYQ036	0.53%Pt-14.3%Co/Al_2O_3	400ºC, flow, 1X	161.6	0.2	4.1	IWI (3X); Condea Vista B, 100-200 mesh
ZYQ037	5%La-15%Co/Al_2O_3	400ºC, flow, 1X	155.1	0.2	3.9	IWI (3X); Condea Vista B, 100-200 mesh
ZYQ038	15%Zr-15%Co/Al_2O_3	400ºC, flow, 1X	160.9	0.1	4.1	IWI (3X); Condea Vista B, 100-200 mesh
ZYQ039	0.2%Re-15%Co/Al_2O_3	400ºC, flow, 1X	156.5	0.2	4.2	IWI (3X); Condea Vista B, 100-200 mesh
ZYQ040	0.5%Re-15%Co/Al_2O_3	400ºC, flow, 1X	136.7	0.2	3.8	IWI (3X); Condea Vista B, 100-200 mesh
ZYQ041	1.0%Re-15%Co/Al_2O_3	400ºC, flow, 1X	187.7	0.2	4.0	IWI (3X); Condea Vista B, 100-200 mesh
ZYQ042	20%Co/ZrO_2-SiO_2	400ºC, flow, 1X	200.0	0.6	8.8	IWI (3X); Davisil 952 SiO_2, 60-80 mesh

Sample ID	Sample Composition	Calcination	BET SA (m_2/g)	+/-	Avg. Pore (nm)	Additional Comments
ZYQ043	0.5%Ru-20%Co/ZrO_2-SiO_2	400ºC, flow, 1X	197.0	0.6	8.4	IWI (3X); Davisil 952 SiO_2, 60-80 mesh
ZYQ044	0.5%Pt-20%Co/ZrO_2-SiO_2	400ºC, flow, 1X	205.5	0.6	9.2	IWI (3X); Davisil 952 SiO_2, 60-80 mesh
ZYQ045	0.5%Re-20%Co/ZrO_2-SiO_2	400ºC, flow, 1X	191.9	0.6	8.9	IWI (3X); Davisil 952 SiO_2, 60-80 mesh
ZYQ050	0.5%Ru-15%Co/Al_2O_3	400ºC, flow, interval 3X	161.0	0.2	3.2	IWI (3X); Davisil 952 SiO_2, 60-80 mesh
ZYQ051	0.2%Re-15%Co/Al_2O_3	400ºC, flow, interval 3X	148.2	0.1	4.0	IWI (3X); Davisil 952 SiO_2, 60-80 mesh
ZYQ052	0.5%Re-15%Co/Al_2O_3	400ºC, flow, interval 3X	151.8	0.1	4.1	IWI (3X); Davisil 952 SiO_2, 60-80 mesh
ZYQ053	2%Re-15%Co/Al_2O_3	400ºC, flow, interval 3X	153.3	0.1	3.9	IWI (3X); Davisil 952 SiO_2, 60-80 mesh
ZYQ054	0.2%Ru-15%Co/Al_2O_3	400ºC, flow, interval 3X	153.8	0.1	4.0	IWI (3X); Davisil 952 SiO_2, 60-80 mesh
ZYQ055	1%Ru-15%Co/Al_2O_3	400ºC, flow, interval 3X	159.1	0.2	3.1	IWI (3X); Davisil 952 SiO_2, 60-80 mesh
LIJ001	10%Co/TiO_2	300ºC, no flow, 1X	---	---	---	IWI: Degussa TiO_2 P25
LIJ002	10%Co-0.1%B/TiO_2	300ºC, no flow, 1X	---	---	---	IWI: Degussa TiO_2 P25
LIJ003	10%Co-0.2%Ru/TiO_2	300ºC, no flow, 1X	---	---	---	IWI: Degussa TiO_2 P25
LIJ004	0.2%Ru-10%Co-0.1%B/TiO_2	300ºC, no flow, 1X	---	---	---	IWI: Degussa TiO_2 P25
LIJ005	10%Co-0.37%Re/TiO_2	300ºC, no flow, 1X	---	---	---	IWI: Degussa TiO_2 P25
LIJ006	10%Co-0.39%Pt/TiO_2	300ºC, no flow, 1X	---	---	---	IWI: Degussa TiO_2 P25

Table 2
Hydrogen Chemisorption and XRD Results

Sample ID	Sample Composition	H_2 Chemisorption % Dispersion	2θ	XRD Co_3O_4 (311) Jade (nm)	XRD Co_3O_4 (311) Winfit (nm)
ZYQ000	15%Co/Al_2O_3	2.40	37.0 (36.9)	18.3 (9.7)	10.3 (6.3)
ZYQ001	15%CoSiO_2	0.85	---	---	---
ZYQ007	0.97%Pt-15%Co/SiO_2	1.24	---	---	---
ZYQ022	15%Co/Al_2O_3	3.03	---	---	---
ZYQ036	0.53%Pt-14.3%Co/Al_2O_3	9.02	37.4 (17.3, 38.6)	13.7 (11.6, 24.5)	9.7 (6.2, 14.4)
ZYQ039	0.2%Re-15%Co/Al_2O_3	7.59 (spent 6.23)	37.0 (36.8, 38.4)	12.5 (6.1, ---)	10.2 (4.9, 20.1)
ZYQ040	0.5%Re-15%Co/Al_2O_3	9.07	---	---	---
ZYQ041	1.0%Re-15%Co/Al_2O_3	9.88 (spent 10.73)	37.1 (37.0, 38.5)	13.0 (8.4)	9.3 (3.3, 32.2)
ZYQ044	0.5%Pt-20%Co/ZrO_2-SiO_2	0.98	---	---	---
ZYQ050	0.5%Ru-15%Co/Al_2O_3	5.00	37.1 (37.1)	---	9.9 (3.0)
ZYQ052	0.5%Re-15%Co/Al_2O_3	5.59	---	---	---
ZYQ053	2%Re-15%Co/Al_2O_3	6.25	---	---	---
ZYQ054	0.2%Ru-15%Co/Al_2O_3	5.58	---	---	---
ZYQ055	1%Ru-15%Co/Al_2O_3	7.11	---	---	---
LIJ001	10%Co/TiO_2	3.64	---	---	---
LIJ002	10%Co-0.1%B/TiO_2	3.19	---	---	---
LIJ003	10%Co-0.2Ru/TiO_2	4.46	---	---	---
LIJ004	0.2%Ru-10%Co-0.1%B/TiO_2	5.12	---	---	---
LIJ005	10%Co-0.37%Re/TiO_2	4.78	---	---	---
LIJ006	10%Co-0.39%Pt/TiO_2	5.11	---	---	---

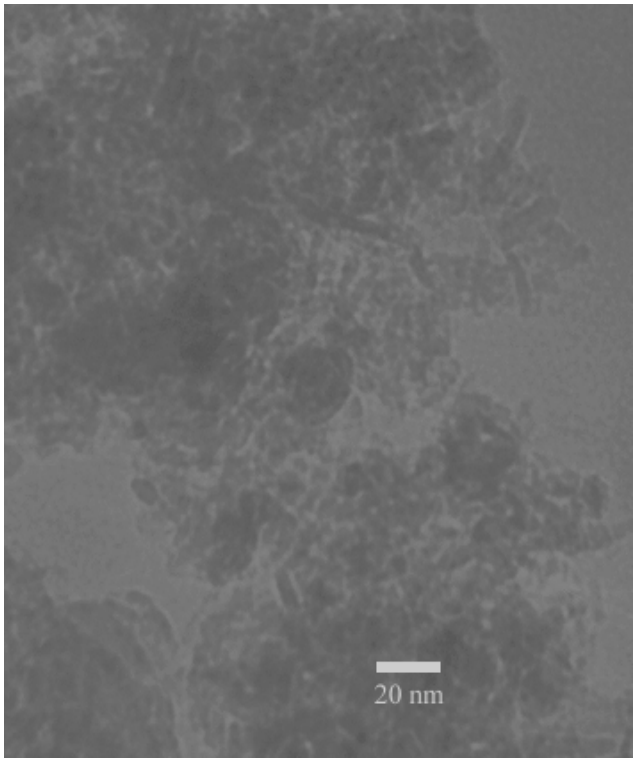

Figure 1a. TEM micrographs for a 0.5% Re promoted 15%Co/Al_2O_3 fresh catalyst.

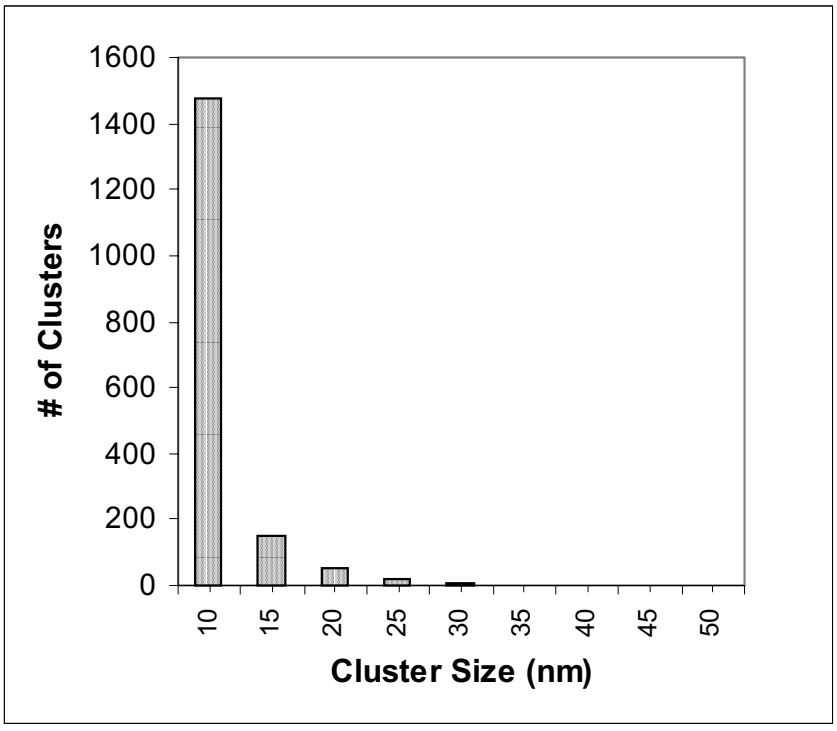

Figure 1b. Particle size distribution from analysis of TEM micrographs for a 0.5% Re promoted fresh 15%$CoAl_2O_3$ catalyst.

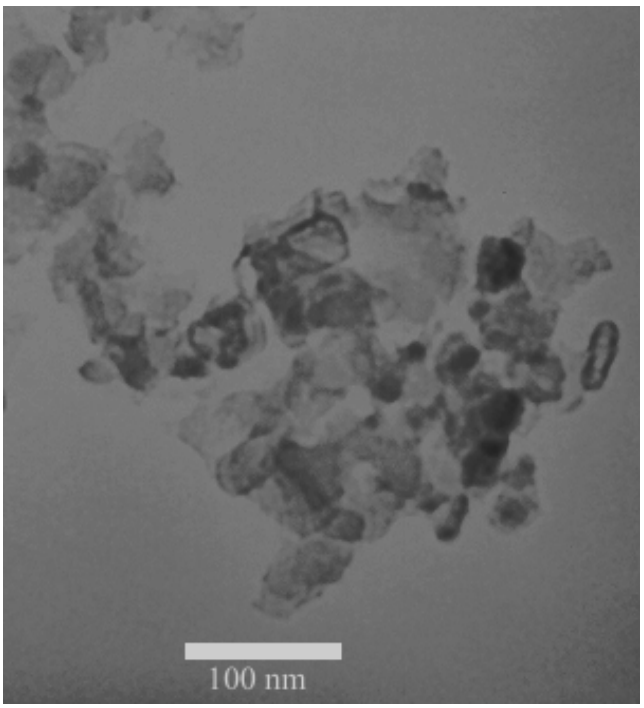

Figure 2a. TEM micrographs for a 0.2% Re promoted 15%Co/Al_2O_3 fresh catalyst.

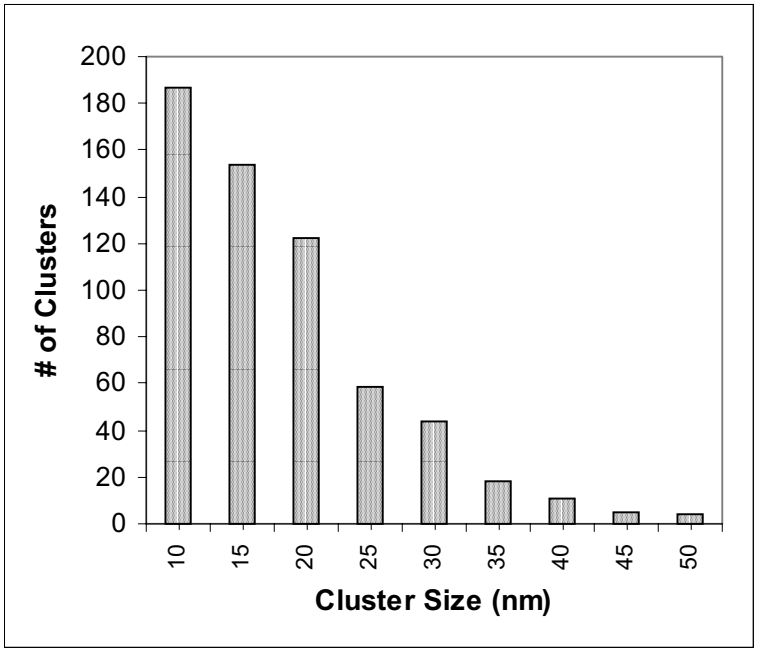

Figure 2b. Particle size distribution from analysis of TEM micrographs for a 0.2% Re promoted 15%Co/Al_2O_3 spent catalyst sampled after reaching a steady-state conversion in the CSTR.

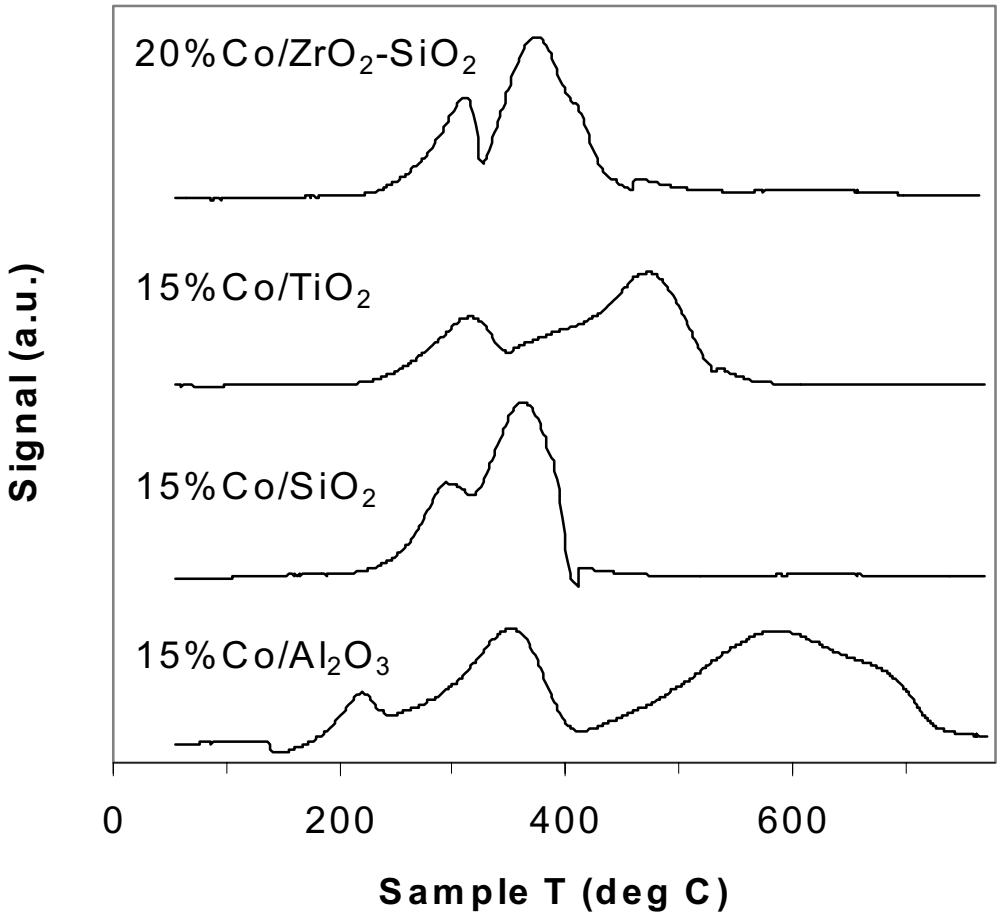

Figure 3. TPR of unpromoted Co catalysts.

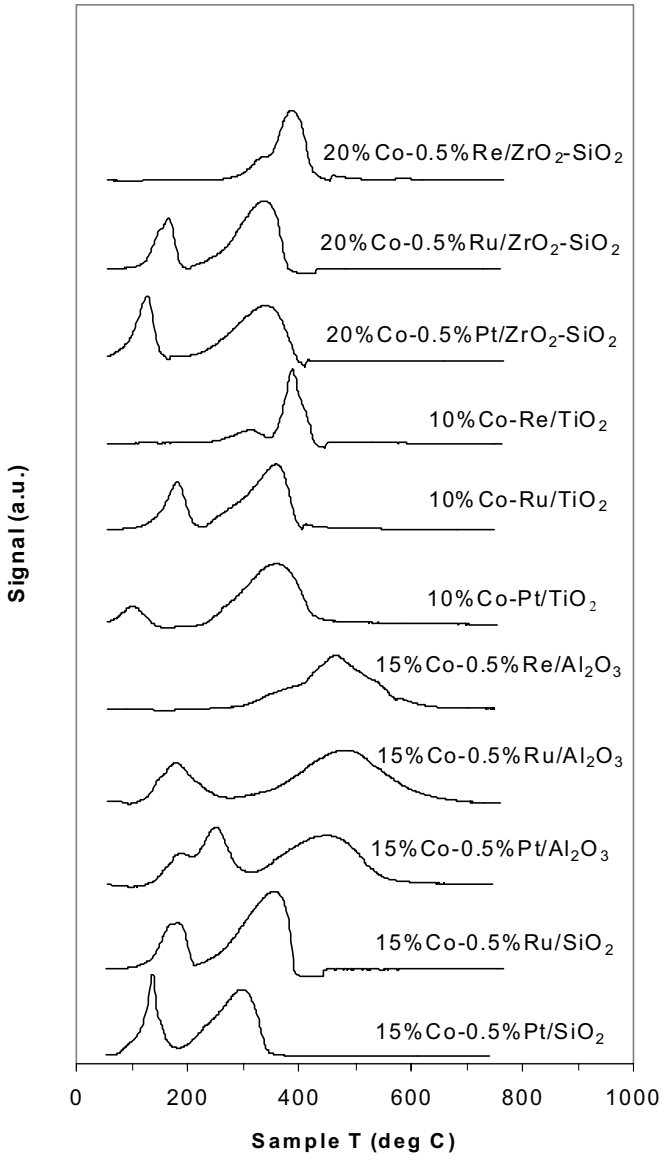

Figure 4. TPR of noble metal promoted Co catalysts.

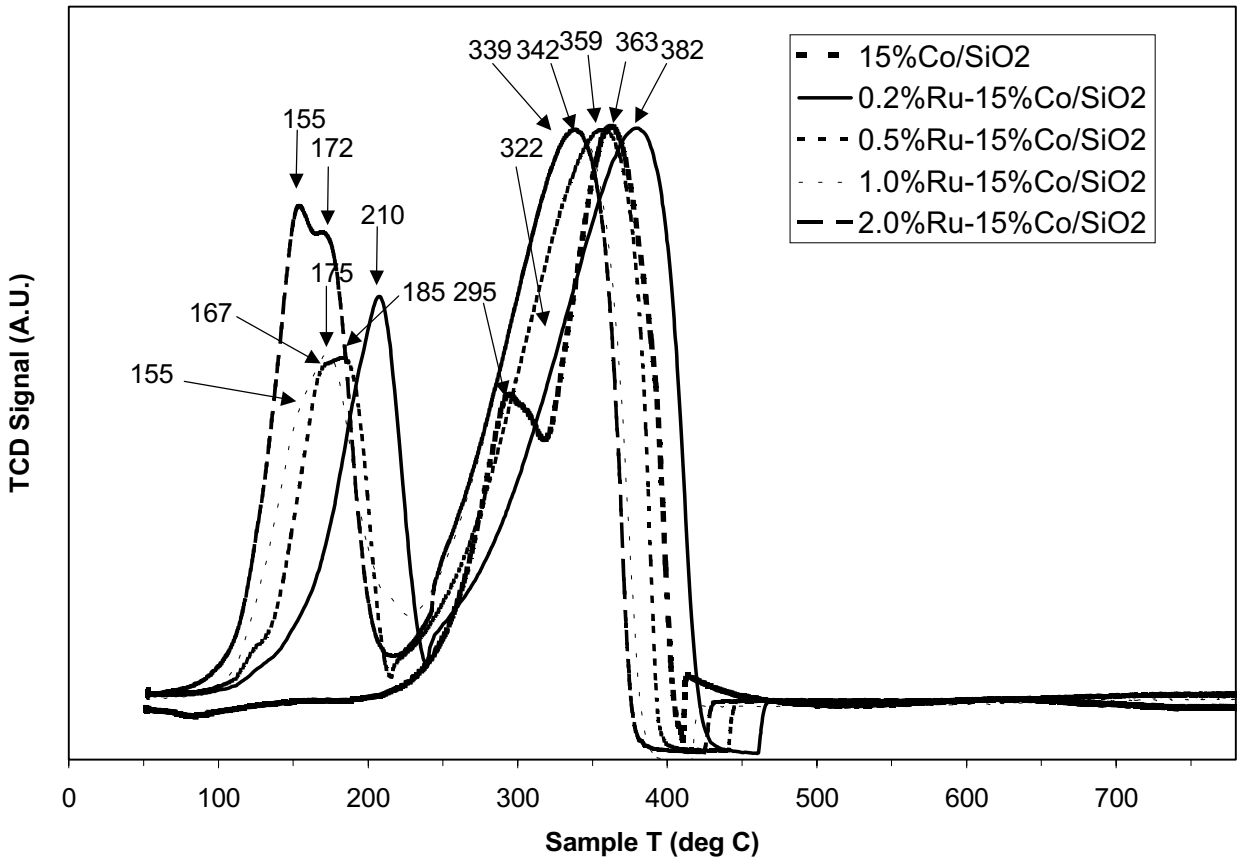

Figure 5. Effect of increasing Ru promoter loading on the reduction temperature of 15%Co/SiO_2.

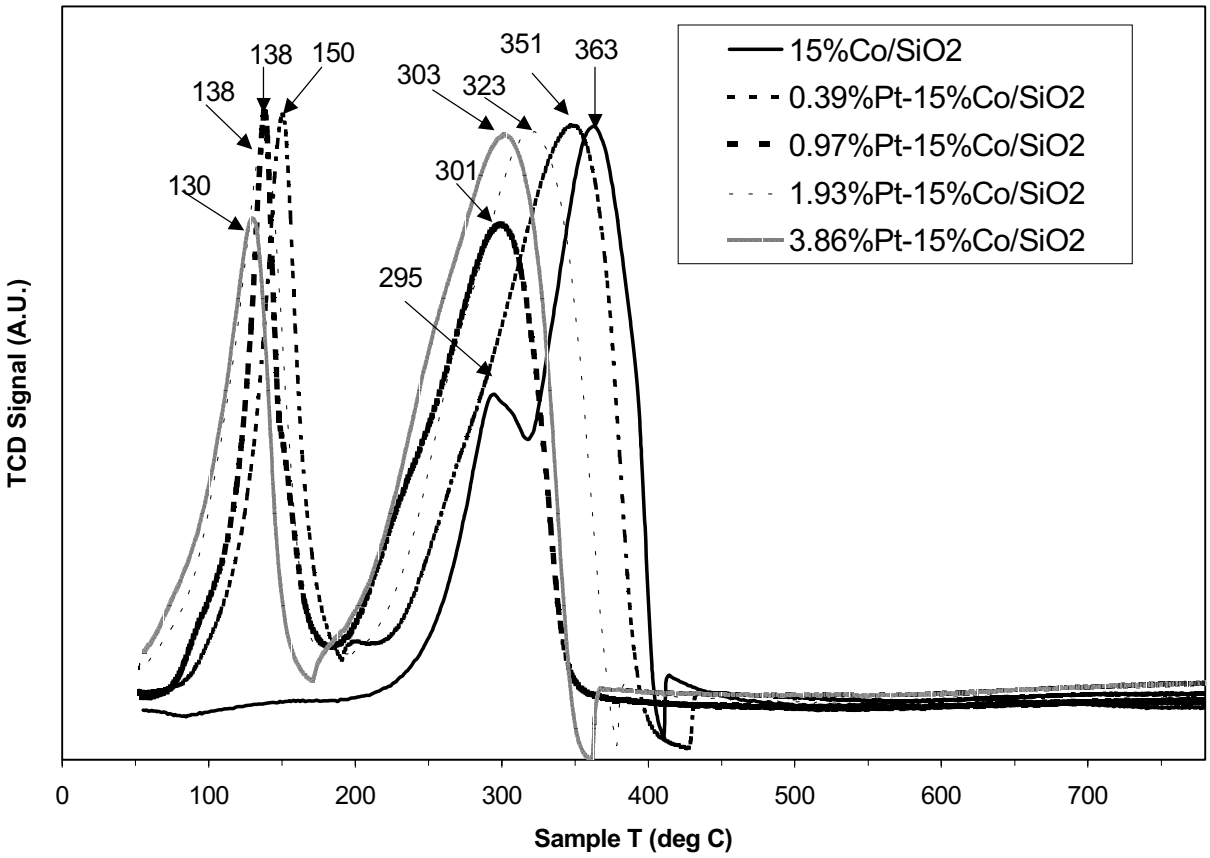

Figure 6. Effect of increasing Pt promoter loading on the reduction temperature of 15%Co/SiO_2.

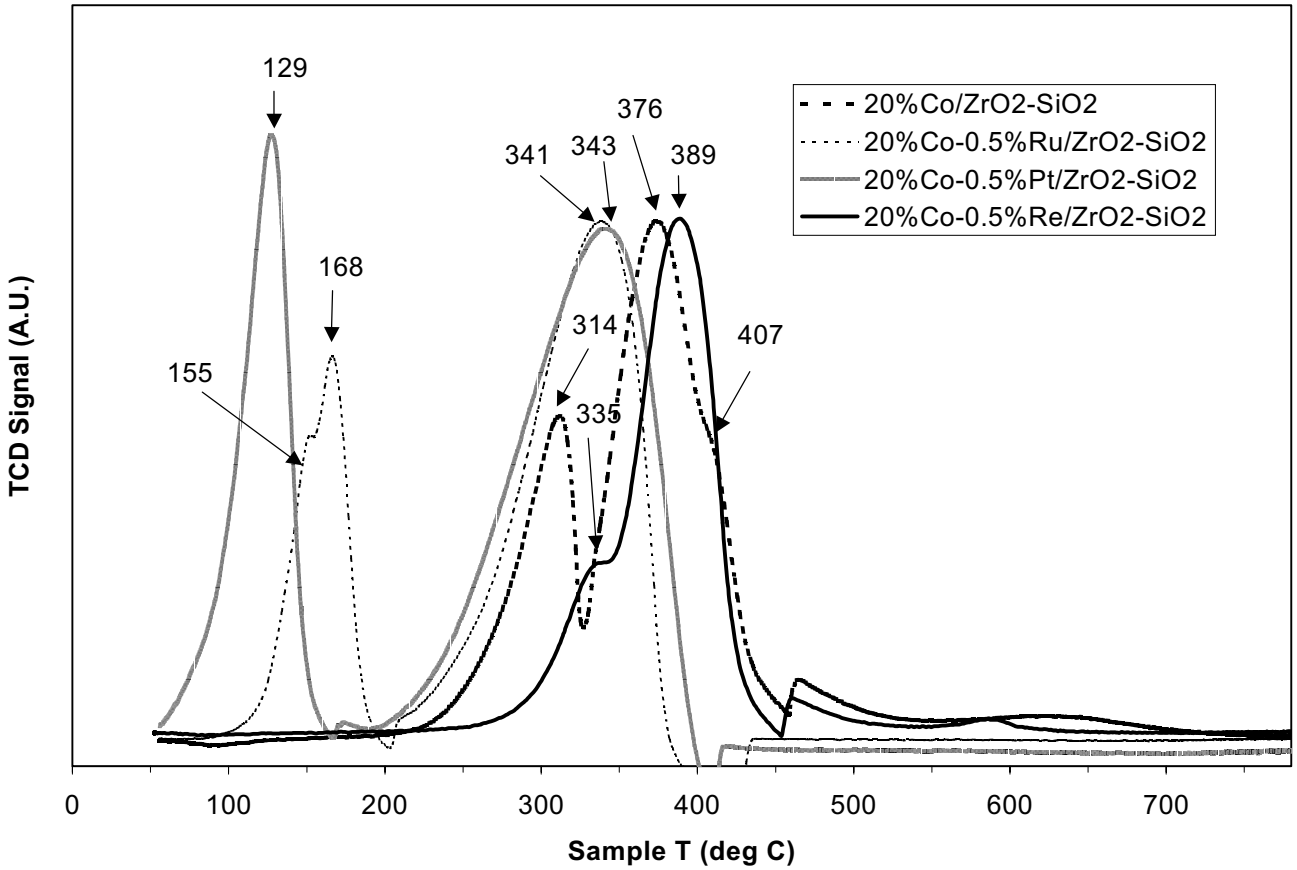

Figure 7. Effect of noble metal promoter type on the reduction temperature of 20%Co/ZrO_2-SiO_2.

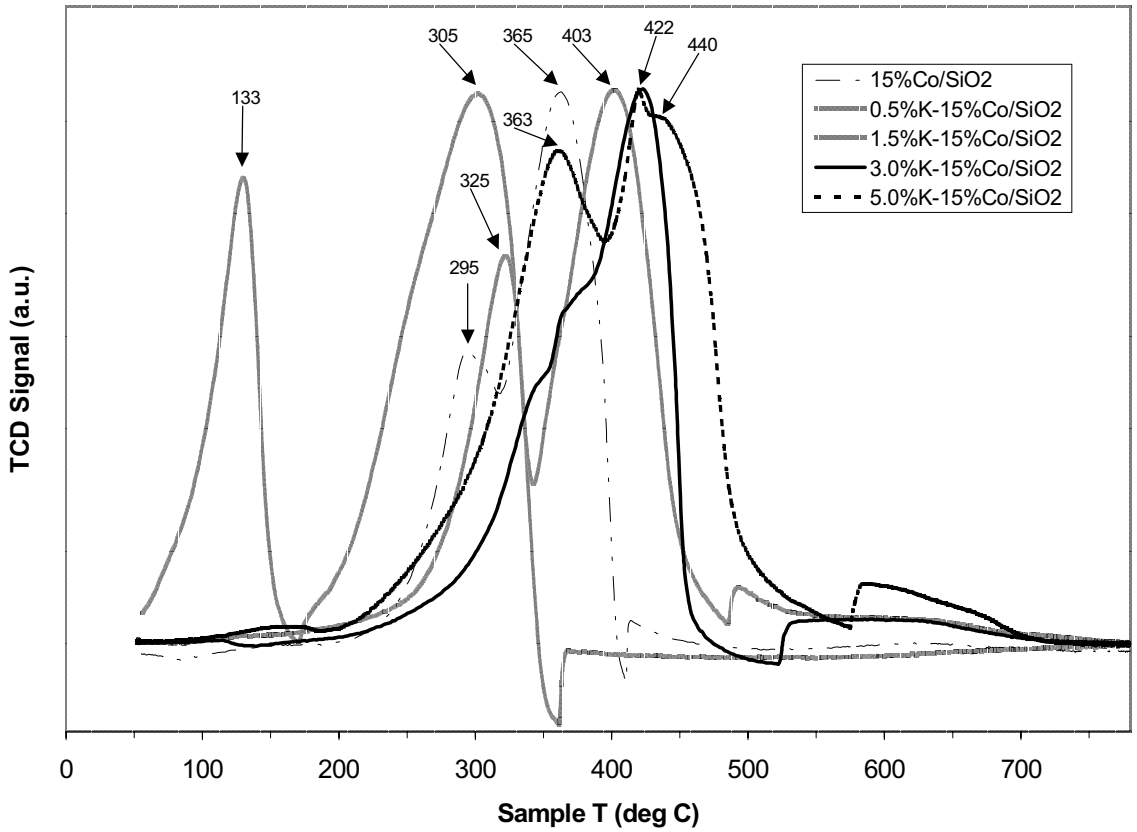

Figure 8. Effect of increasing K additive loading on the reduction temperature of 15%Co/SiO_2.

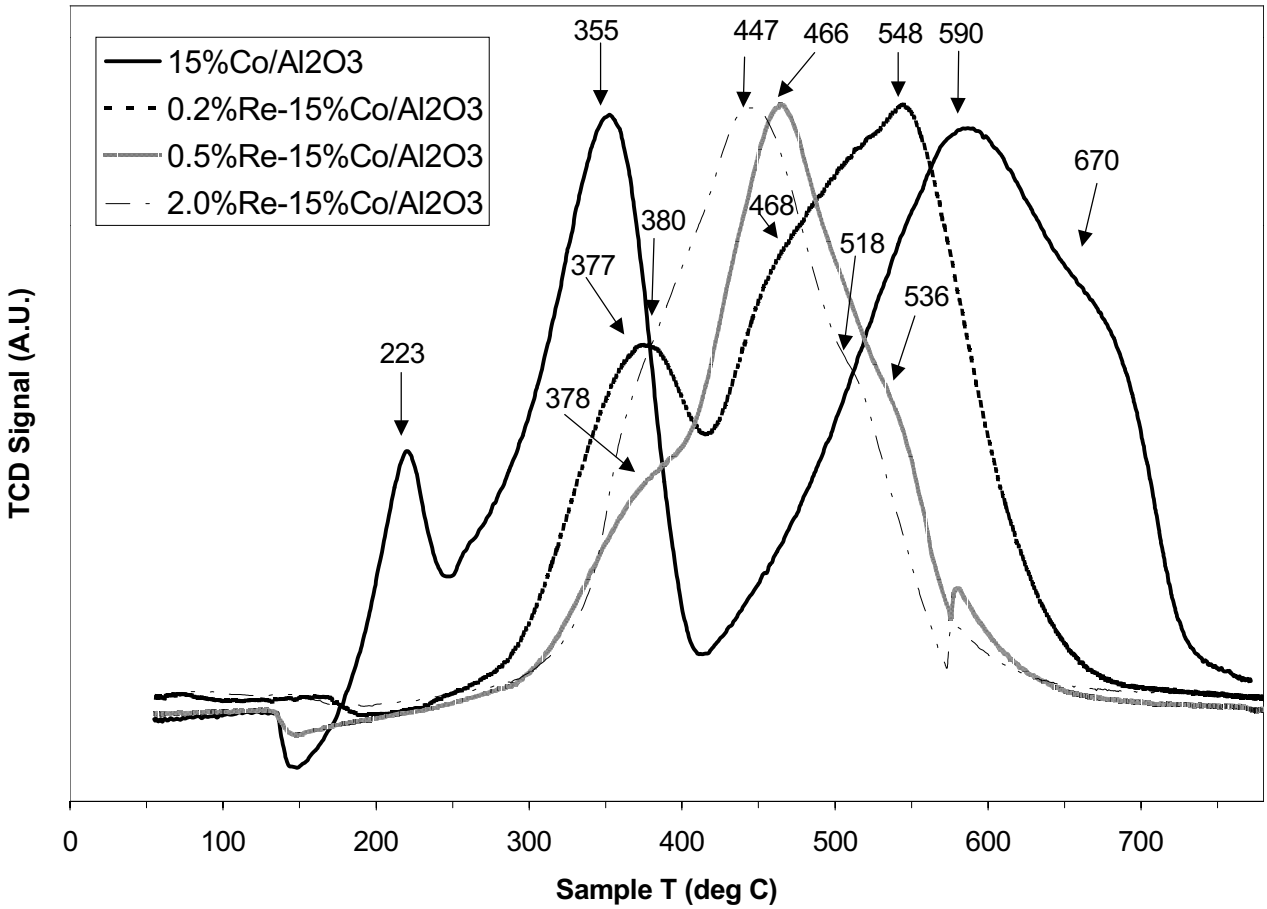

Figure 9. Effect of increasing Re promoter loading on the reduction temperature of 15%Co/Al_2O_3 (three interval drying steps and one final calcination step).

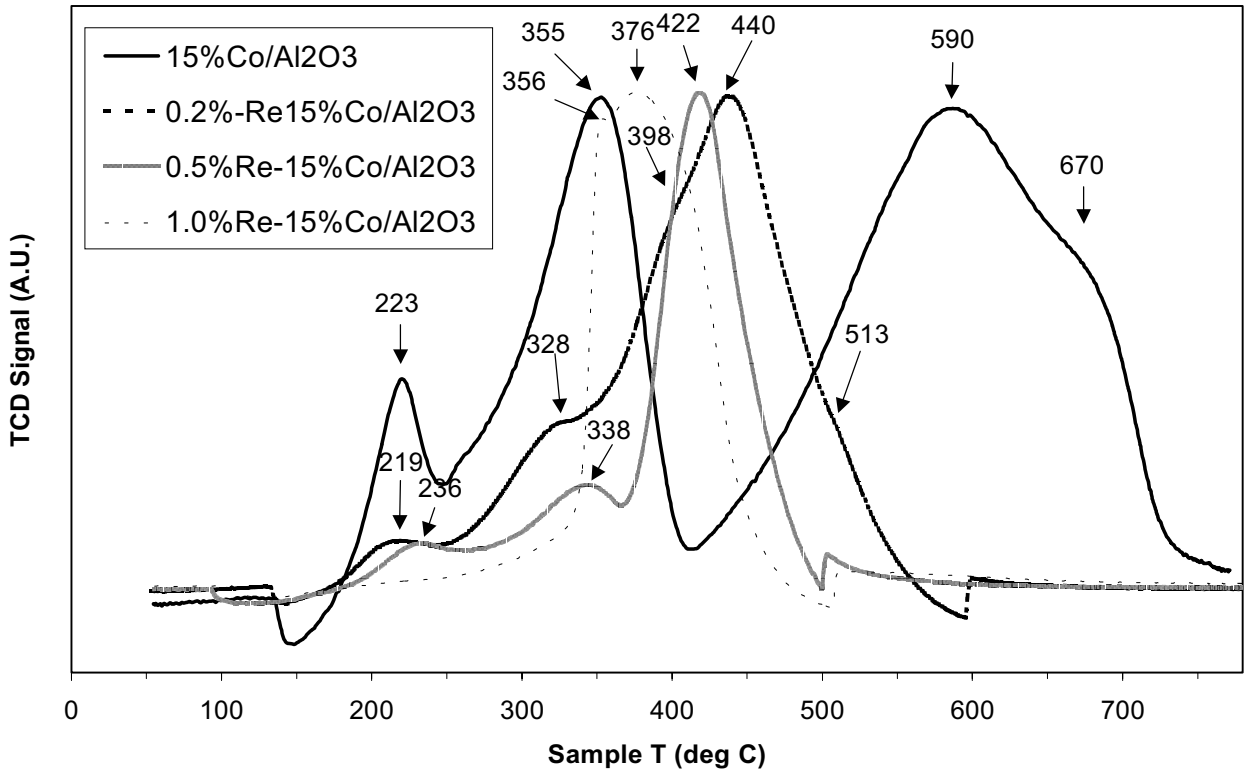

Figure 10. Effect of increasing Re promoter loading on the reduction temperature of 15%Co/Al_2O_3 (three interval drying steps and three interval calcination steps).

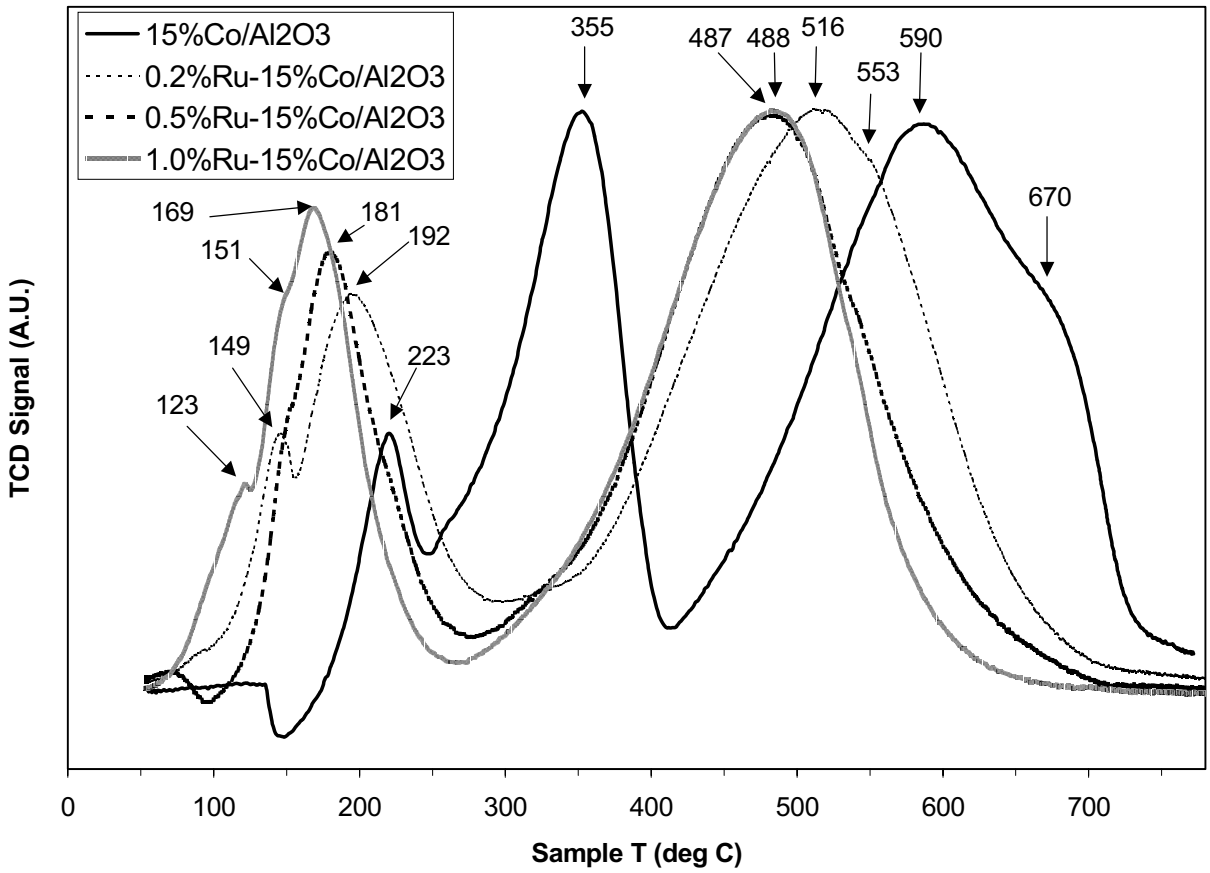

Figure 11. Effect of increasing Ru promoter loading on the reduction temperature of 15%Co/Al_2O_3.

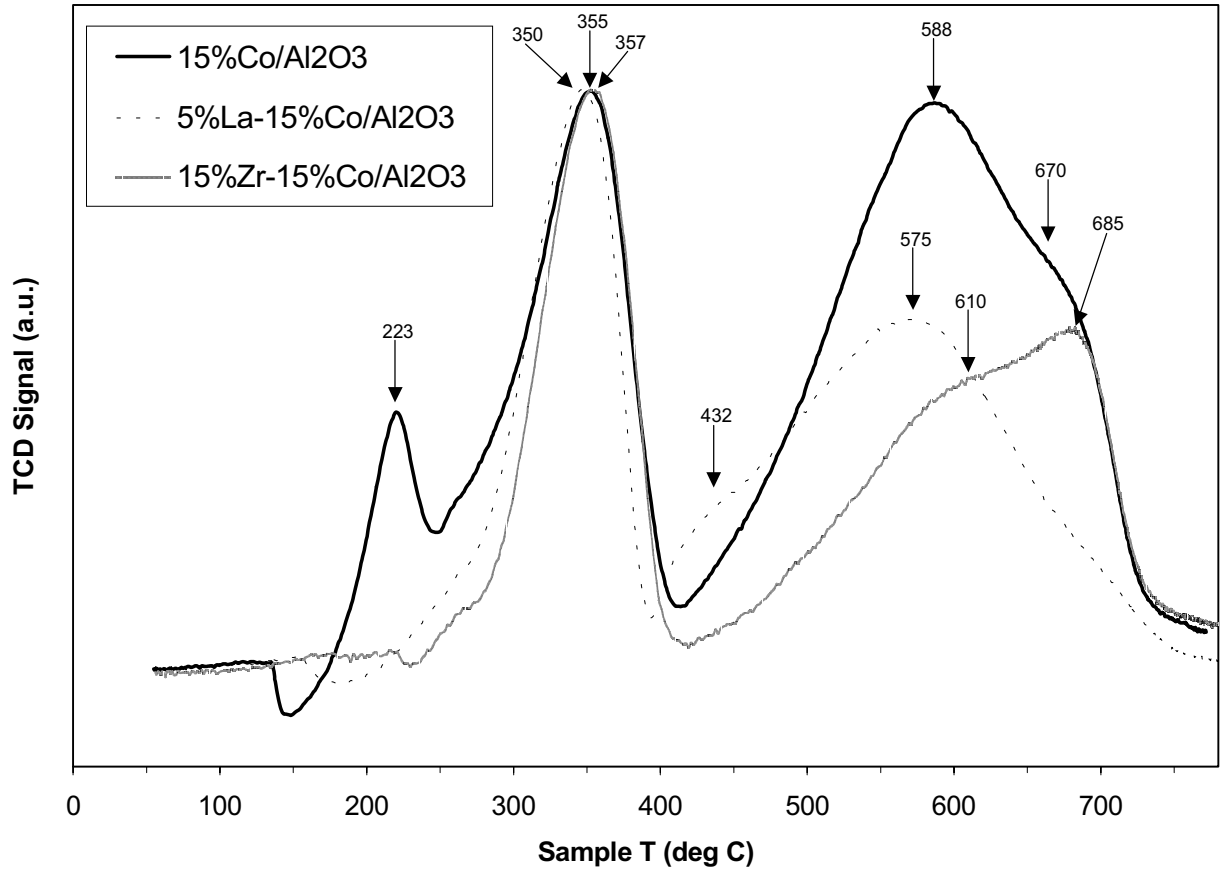

Figure 12. Effect of La or Zr additive on the reduction temperature of 15%Co/Al_2O_3.

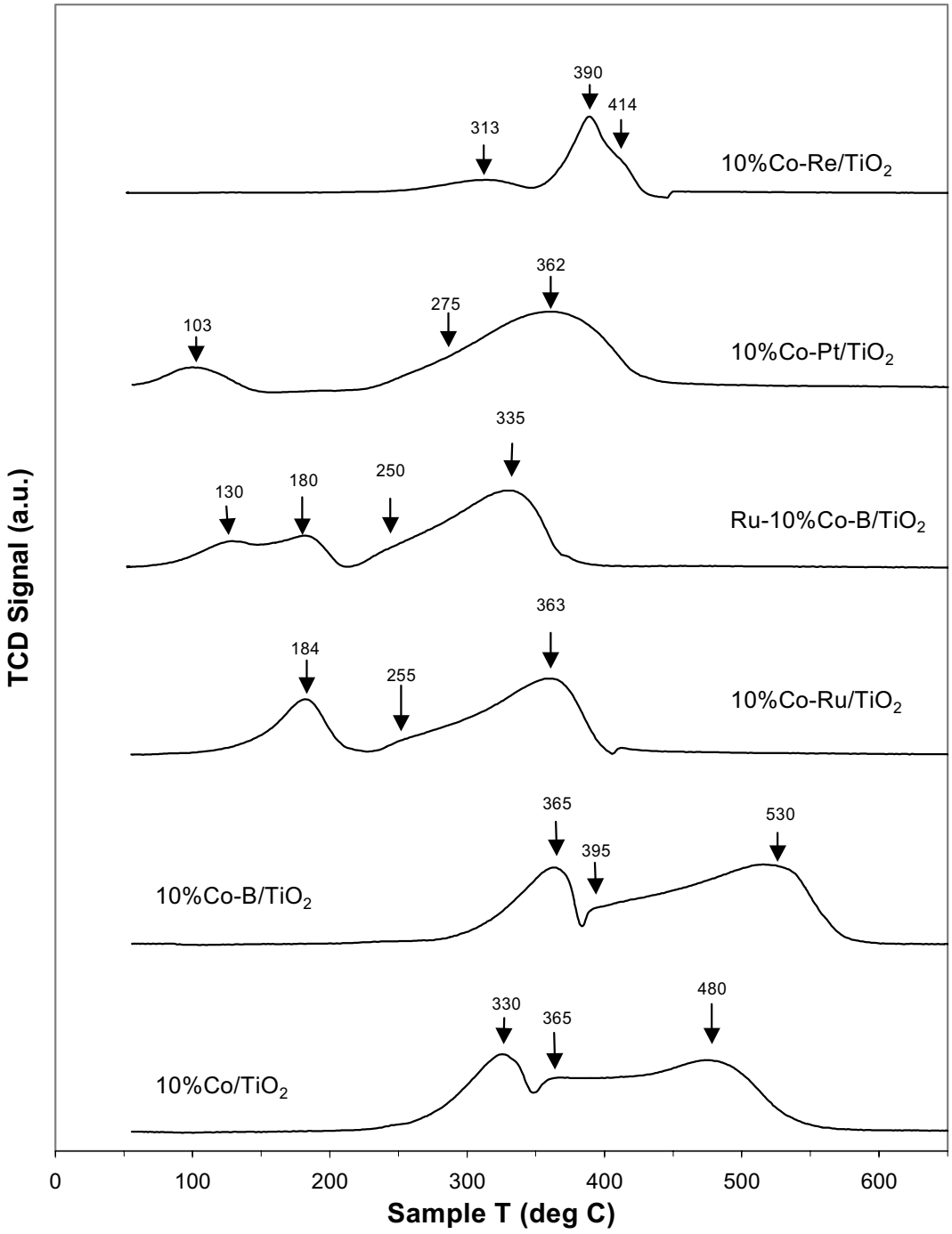

Figure 13. Effect of promoter addition on the reduction temperature of 10%Co/TiO_2.

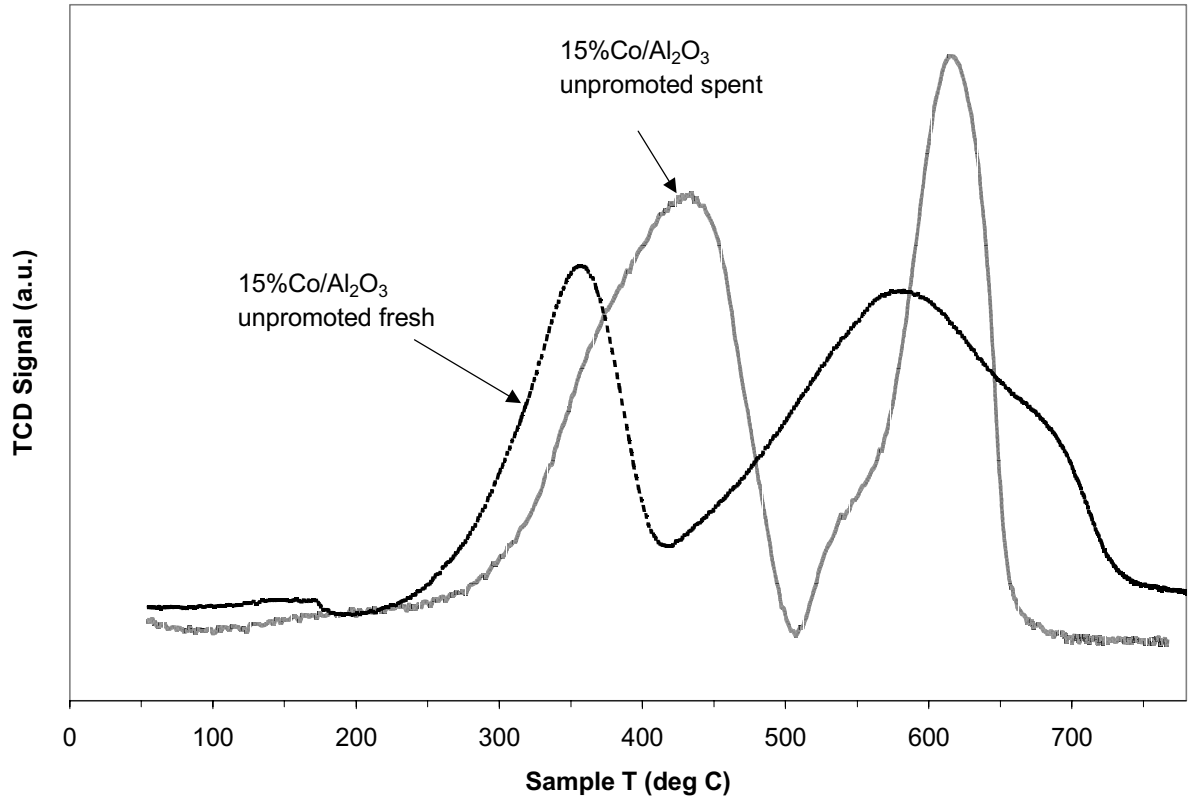

Figure 14. TPR profiles of fresh and spent unpromoted 15%Co/Al_2O_3 catalysts.

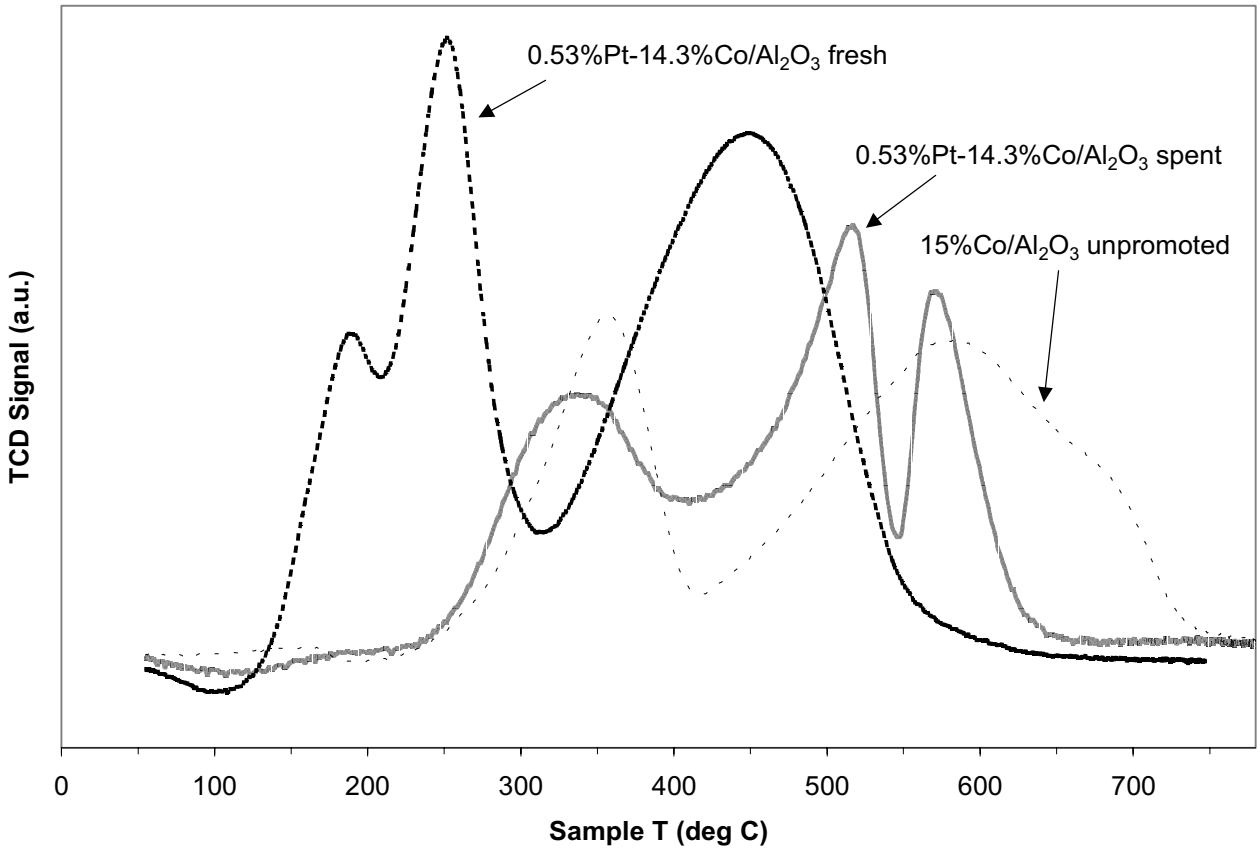

Figure 15. TPR profiles of fresh and spent 14.3%Co/Al_2O_3 catalysts promoted by 0.53% Pt referenced to the unpromoted fresh 15%Co/Al_2O_3 catalyst.

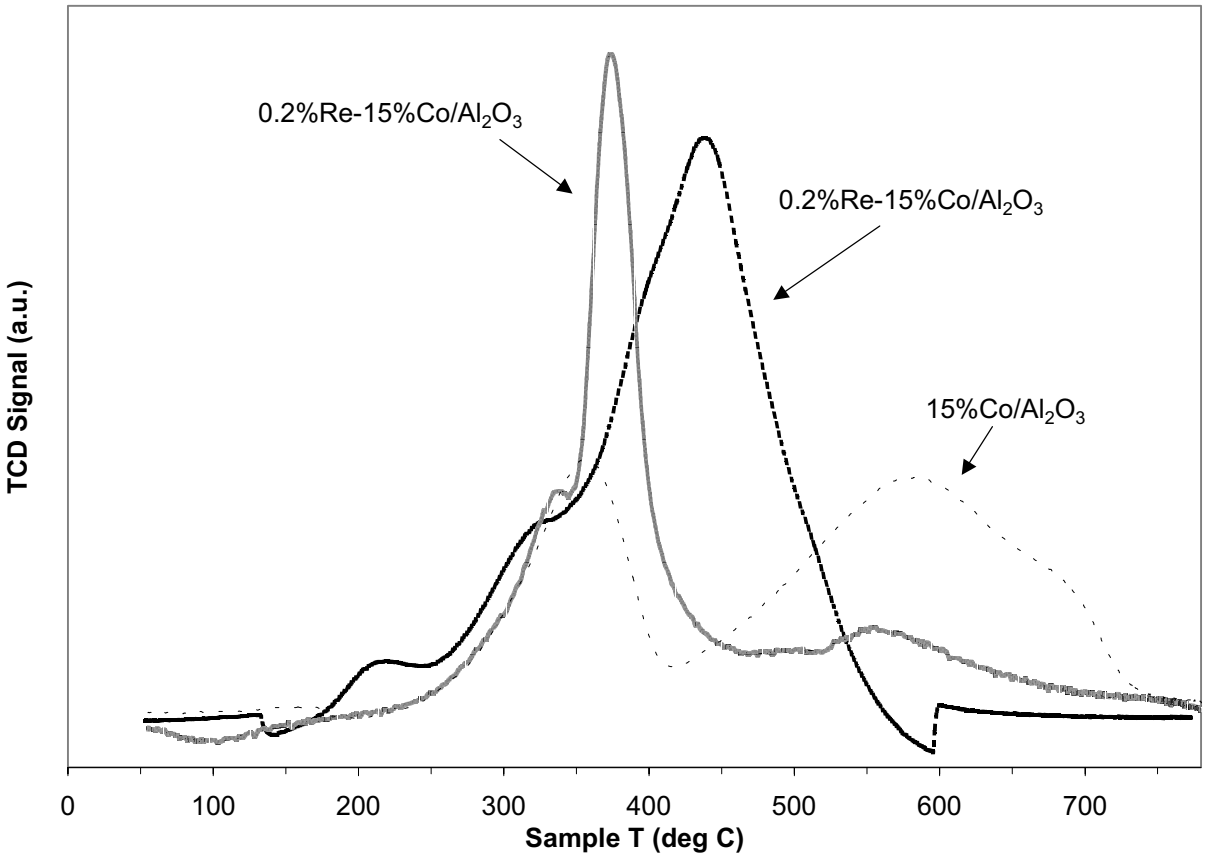

Figure 16. TPR profiles of fresh and spent 15%Co/Al_2O_3 catalysts promoted by 0.2% Re referenced to the unpromoted fresh 15%Co/Al_2O_3 catalyst.

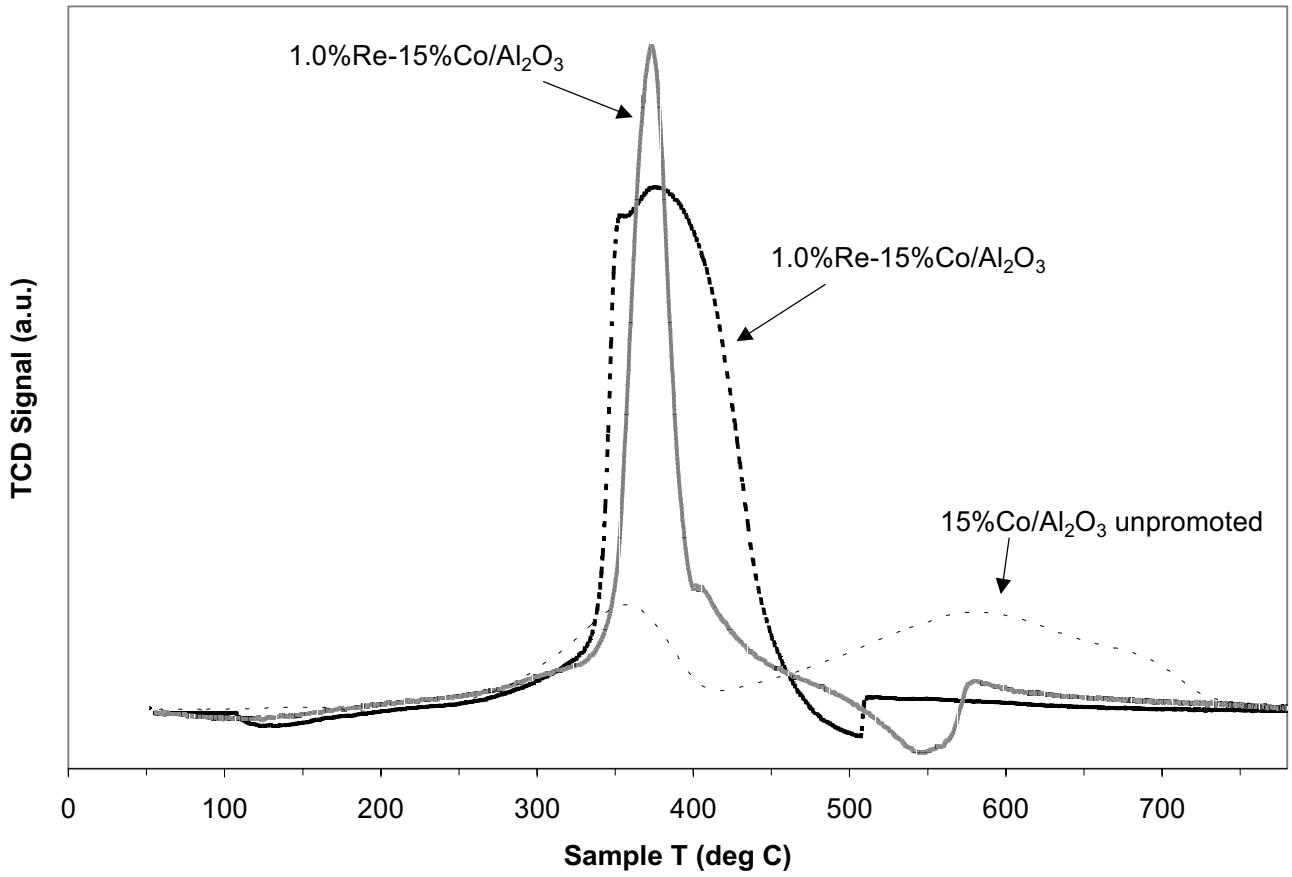

Figure 17. TPR profiles of fresh and spent 15%Co/Al_2O_3 catalysts promoted by 0.2% Re referenced to the unpromoted fresh 15%Co/al_2O_3 catalyst.

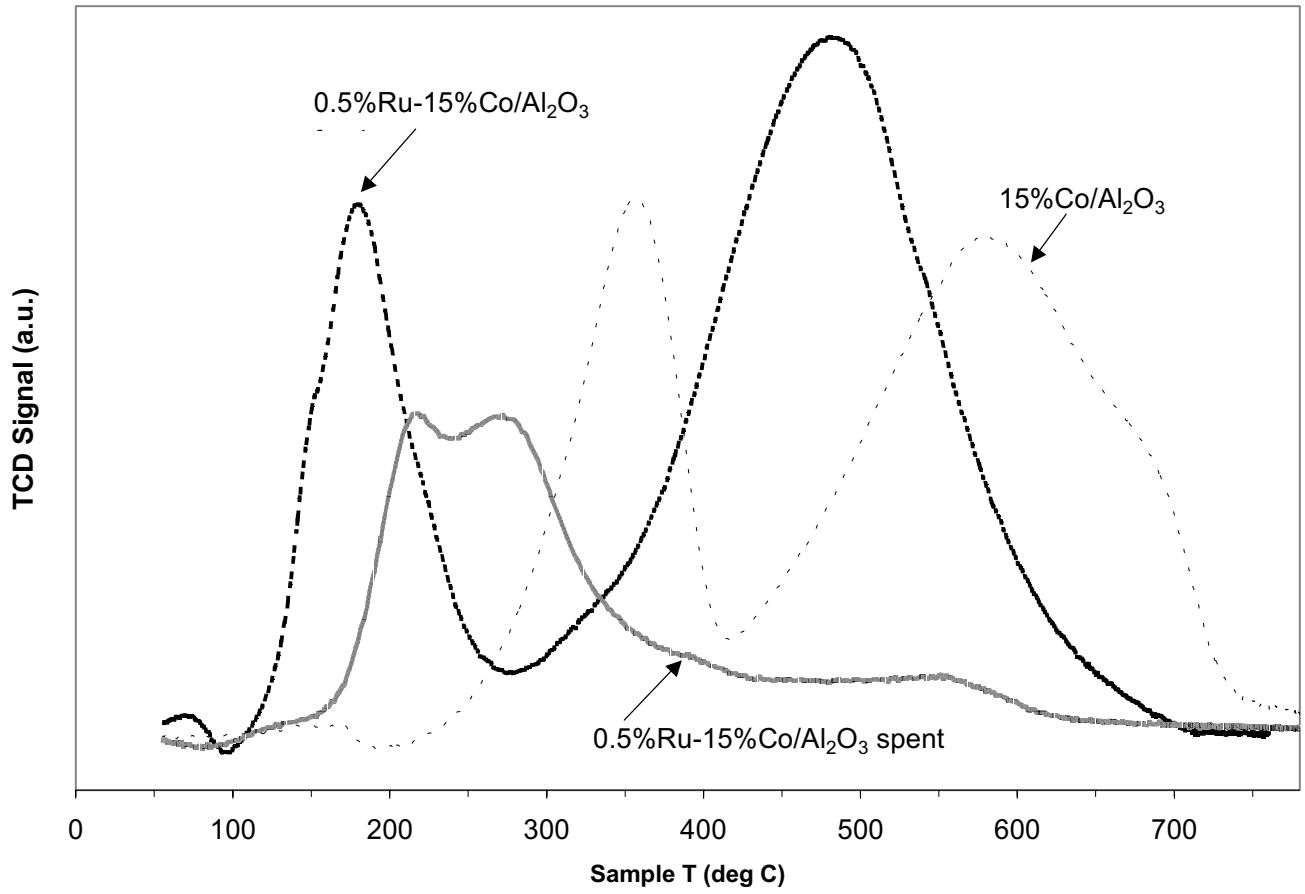

Figure 18. TPR profiles of fresh and spent 15%Co/Al_2O_3 catalysts promoted by 0.5% Ru referenced to the unpromoted fresh 15%Co/Al_2O_3 catalyst.

Task 4. Wax/Catalyst Separation

The objective of this task is to develop techniques for the separation of catalysts from FT reactor slurries.

A. Slurry Bubble Column Reactor (SBCR) Activities

Abstract

The following discussion describes the work done to enhance the CAER's SBCR system. A 5.08 cm diameter by 2 m tubular reactor had been modified to operate in a Fischer-Tropsch SBCR mode. The previous work had focused primarily on catalyst separation from the wax products. Problems with maintaining a constant catalyst inventory within the reactor have been addressed and design modifications are underway. Heat load/loss calculations have been performed to evaluate the need for cooling with high space velocities.

Introduction

Current SBCR Configuration

Currently, the CAER is utilizing the Prototype Integrated Process Unit (PIPU) system for scale-up research of the Fischer-Tropsch Synthesis (FTS).

The PIPU is a pilot plant system built in the early 1980s for studying a multitude of synthetic fuel/chemical processes. In the mid 1990s, a direct coal liquefaction reactor within the PIPU plant was reconfigured as a SBCR for FTS studies (see Figure 1.). The reactor was originally designed to operate with coarse catalyst pellets (>500 μm). Consequently, the reactor system did not contain a wax separation system sufficient for smaller catalyst particles that are typically used in FTS. Therefore, a slurry accumulator and a batch wax filtration system were installed.

The bubble column reactor has 5.08 cm diameter and a 2 m height with an effective reactor volume of 4 liters. The synthesis gas was passed continuously through the reactor. The product gas and liquid exit the top of the reactor and pass through a separation section to a hot condenser (230^{o}C), and a cold separator (3^{o}C). Product wax was batch filtered from the accumulator vessel. A dry flow meter for SBCR was used to measure the exit gas flow rate. A more detailed description of the SBCR was described in the previous final report (ref. 1).

Early attempts to operate the reactor in a F-T mode were successful in that a clear wax product could be obtained. The iron concentration in the wax collected after passing the separation system in the SBCR was about 10 ppm. The initial activity observed in the bubble column was about 10% less than that of comparable CSTR runs. In addition, the rate of conversion decline in the SBCR was much greater than that observed in the CSTR.

This apparent increased deactivation rate in the SBCR may be due to the nature of the wax/catalyst separation system and the physical limitations for controlling the distribution of the catalyst particles between the reactor and a slurry receiver vessel placed overhead. The volume of the overhead receiving vessel (18 L), containing unfiltered wax, is relatively large as compared with the reactor vessel volume (about 4 L). Gas and entrained slurry exit the top of the reactor and are collected in the 18 L vessel. Unfiltered slurry recirculates via a natural convection loop through a dip-tube located inside the reactor. At least 8 liters of slurry must accumulate in the receiver vessel before the wax could be batch-filtered from the catalyst using a Mott sintered-metal filtration tube. This effectively lowers the concentration of catalyst in the reactor slurry phase and thereby increases the space velocity over the course of a run.

Proposed SBCR Modifications

Since we focused primarily on small-scale 1-liter CSTR reactor studies in the last five years, solving the above-mentioned problem with the SBCR had not been a priority. Recently however, industrial involvement regarding catalyst attrition studies, catalyst/wax separation, and bulk wax sample production has renewed interest in operating the SBCR system. Therefore, we are currently making design changes to the catalyst/wax separation system so that the volume of slurry within the SBCR remains at equilibrium. In addition, we are modifying the filtration system to accept a variety of filter elements.

Based on our analysis of previous SBCR runs, the following design objectives were decided upon for enhancing the operation of the SBCR:

1. The level of slurry in the overhead tank should be controlled and quantified so that the amount of catalyst inside the reactor can be accurately estimated;
2. The volume of unfiltered slurry outside the reactor should be minimized; and
3. The modified system should be able to accept a variety of commercially available filter systems.

The proposed design modifications for meeting these objectives are shown schematically in Figure 2. Gas and slurry exit through a port near the top of the reactor column. The slurry will be disengaged from the gas phase in an overhead receiver with a volume of about 4 liters. The level or volume of the slurry within the receiver will be continuously monitored by measuring the differential pressure across the height of the vessel. An argon purge of both pressure legs will keep the lines free of slurry. The volume of slurry within the receiver will be controlled to be no more than 1 liter by removing wax from the reactor system via a control valve. Filtered wax will be held in a heated 18 liter storage vessel. The unfiltered slurry will flow back to the reactor via

a natural convection loop through a dip-tube exiting near the bottom of a reactor. The filter assemble will be located outside the overhead receiver so that changes in the filter media can be made on-line, without aborting or interrupting the reactor run.

Heat Loss Analysis Results

Previously, the SBCR was operated with a slurry catalyst concentration less than 20% and space velocities lower than 5 slpm/g. Since the current reactor configuration does not include a heat removal system, the heat load at higher space velocities (and slurry concentration > 20 wt%) may exceed the heat loss to the surroundings. This is a concern since the small reactor diameter (5.08 cm) limits the placement of internal heat transfer surfaces.

The system heat load due to the heat of reaction was calculated based on a $CO+H_2$ conversion ranging from 70 to 80%. The heat loss was estimated by considering both radiative and convective cooling using the method of Kern (ref.2) for the ideal case of an well-insulated vertical pipe. Results of the heat transfer analysis for operating with a 30 wt% slurry are shown in Figure 3. The point of zero heat load (i.e., when the heat generation is equal to the convective and radiative heat losses) occurs at a space velocity of 2 slpm/g. Therefore, for space velocities greater than 2 slpm/g, heat must be removed and conversely for space velocities less than 2 slpm/g, the heat must be added to the SBCR to maintain a constant temperature.

In reality, the SBCR heat loss may be greater than that of a well-insulted pipe since the reactor is only partially covered with the heating mantel. Thus, the above analysis should be considered a conservative estimate. However, the analysis does indicate that some means of cooling the reactor may be required for high space velocities and conversions. Cooling the reactor vessel shell is not practical because the coils would interfere with the heating mantel used during the initial start-up periods. Cooling surfaces mounted between the mantel and the reactor

could result in localized hot-spots and potentially ruin the heating elements. Since internal cooling is not practical in this case, external cooling of the slurry is being considered. One practical option is to cool the slurry in the overhead accumulator before returning the SBCR.

Conclusions

Once the proposed modifications are implemented, the overall performance of the CAER SBCR will be improved. The reactor slurry level control system will improve the stability of long-duration catalyst deactivation experiments. External slurry filtration will allow for changes in filter media during reactor runs with minimal process upsets. In addition, the design improvements will allow for a more accurate comparison of catalyst performance in the bubble column and CSTR reactors.

References

1. Davis, B. H., Technology Development for Iron Fischer-Tropsch Catalysis, Final Report, DE-AC22-94PC94055, 1997.
2. Kern, D., *Process Heat Transfer*, McGraw-Hill Book Company, 1950.

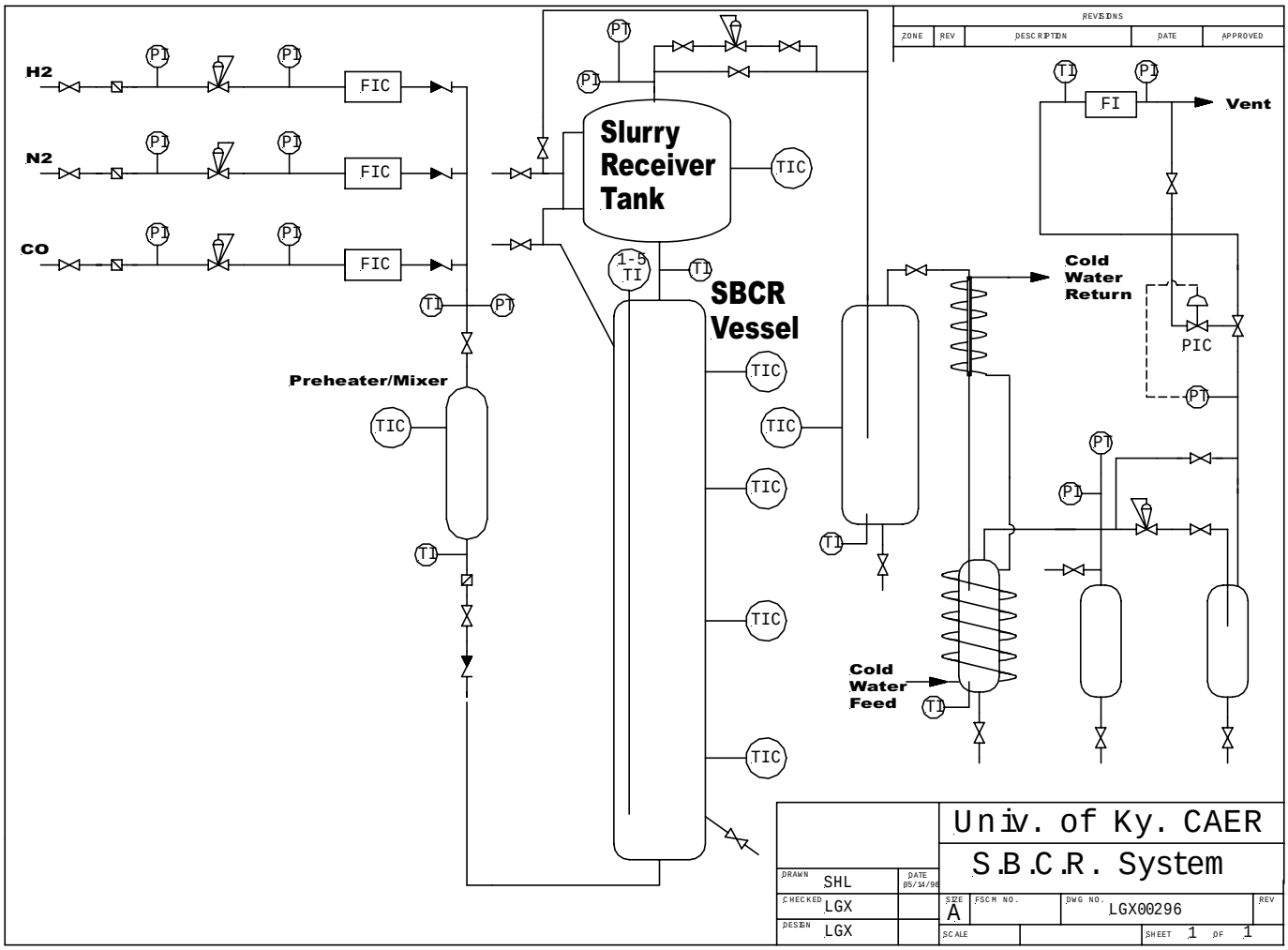

Figure 1. CAER 2" i.d. slurry bubble column reactor system.

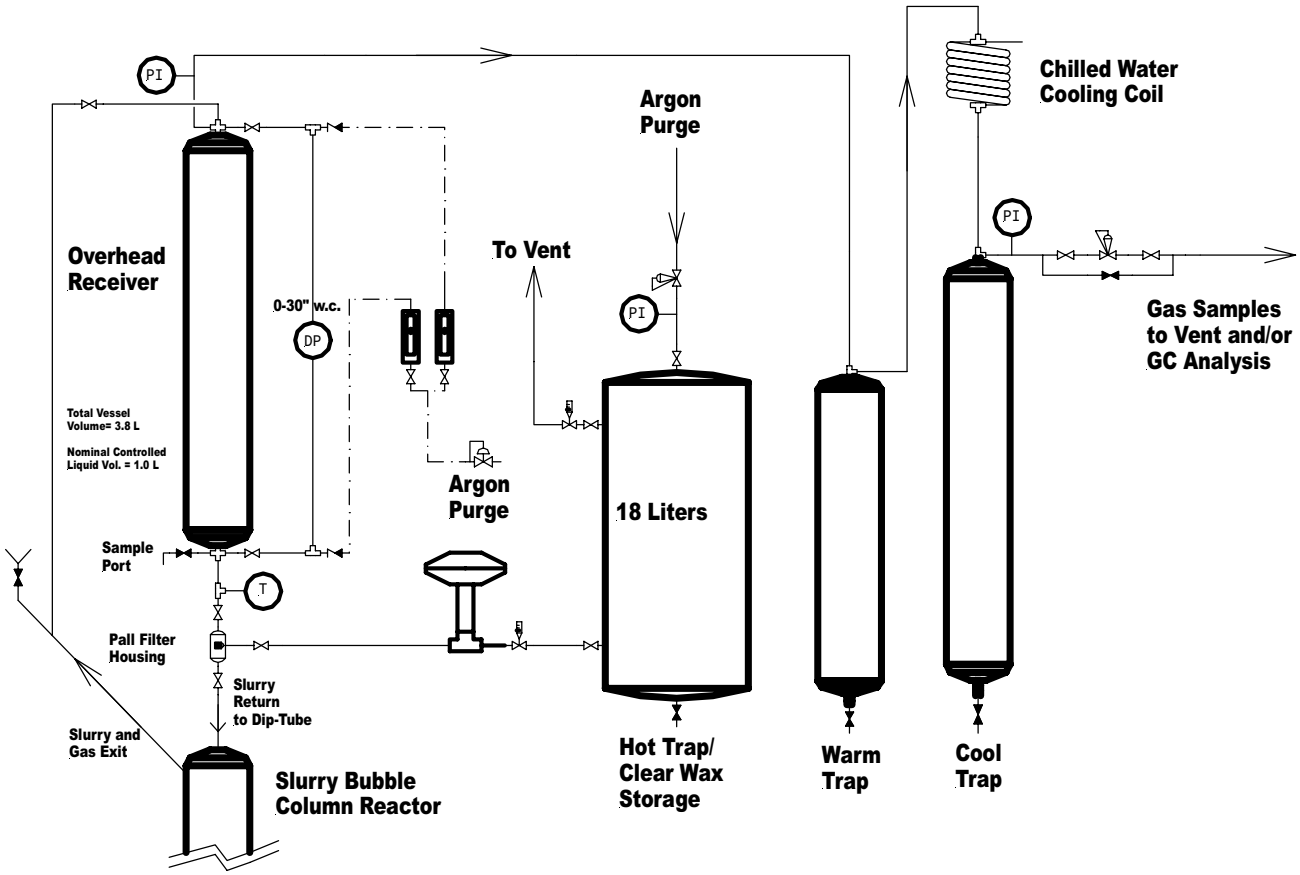

Figure 2. Modified SBCR wax/catalyst separation and sample collection systems.

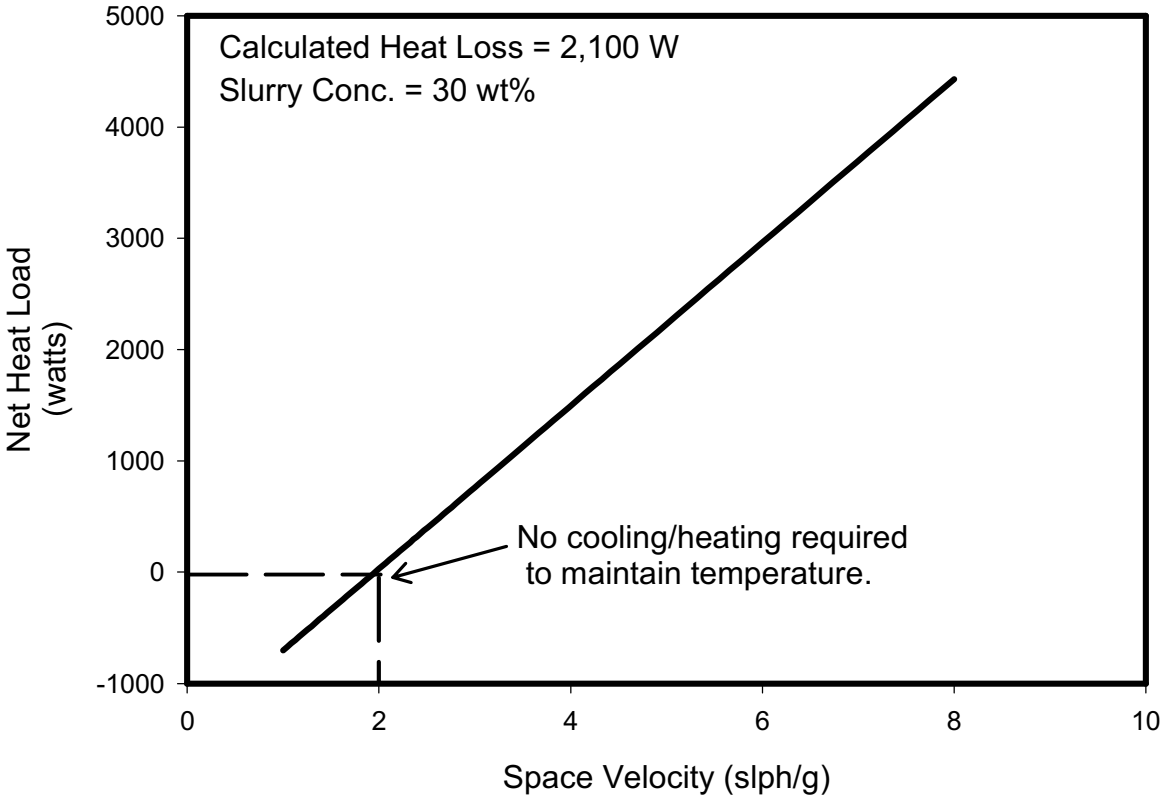

Figure 3. CAER 2" (5.08 cm) i.d. SBCR: effect of space velocity on net heat load.